© 2021. Published by The Company of Biologists Ltd | Development (2021) 148, dev199399. doi:10.1242/dev.199399

RESEARCH ARTICLE

Initiation of *Otx2* expression in the developing mouse retina requires a unique enhancer and either *Ascl1* or *Neurog2* activity

Michael L. Kaufman[1], Noah B. Goodson[1], Ko Uoon Park[1], Michael Schwanke[1], Emma Office[1], Sophia R. Schneider[1], Joy Abraham[1], Austin Hensley[1], Kenneth L. Jones[2] and Joseph A. Brzezinski[1,*]

ABSTRACT

During retinal development, a large subset of progenitors upregulates the transcription factor *Otx2*, which is required for photoreceptor and bipolar cell formation. How these retinal progenitor cells initially activate *Otx2* expression is unclear. To address this, we investigated the *cis*-regulatory network that controls *Otx2* expression in mice. We identified a minimal enhancer element, DHS-4D, that drove expression in newly formed OTX2+ cells. CRISPR/Cas9-mediated deletion of DHS-4D reduced OTX2 expression, but this effect was diminished in postnatal development. Systematic mutagenesis of the enhancer revealed that three basic helix-loop-helix (bHLH) transcription factor-binding sites were required for its activity. Single cell RNA-sequencing of nascent *Otx2*+ cells identified the bHLH factors *Ascl1* and *Neurog2* as candidate regulators. CRISPR/Cas9 targeting of these factors showed that only the simultaneous loss of *Ascl1* and *Neurog2* prevented OTX2 expression. Our findings suggest that *Ascl1* and *Neurog2* act either redundantly or in a compensatory fashion to activate the DHS-4D enhancer and *Otx2* expression. We observed redundancy or compensation at both the transcriptional and enhancer utilization levels, suggesting that the mechanisms governing *Otx2* regulation in the retina are flexible and robust.

KEY WORDS: Enhancers, *Cis*-regulation, Retinal development, Otx2, Ascl1, Neurog2

INTRODUCTION

The retina is a complex multi-layered tissue that comprises seven major cell types, six neuronal and one glial. These retinal cell types arise from a common pool of undifferentiated progenitors in an order relative to the timing of permanent cell cycle exit, that is, their birthdate (Turner and Cepko, 1987; Turner et al., 1990). The early-born cell types include ganglion cells, amacrines, horizontals and cone photoreceptors, whereas rod photoreceptors, bipolar cells and Müller glia are primarily born late in development (Carter-Dawson and LaVail, 1979; la Vail et al., 1991; Rapaport and Vietri, 1991; Wong and Rapaport, 2009; Young, 1985). This commitment of cell-type identities is a crucial early event that establishes unique gene expression networks that underlie cell type-specific functions. The gene regulatory networks that control retinal cell fate commitment events are only partially understood.

Transcription factors play a major role in entrenching cell-fate choices within the retina. The homeobox transcription factor *Otx2* is highly involved in retinal neurogenesis. *Otx2* expression begins around embryonic day (E) 12, correlating with the earliest birthdates of photoreceptors (Nishida et al., 2003). *Otx2* becomes upregulated in a large subset of progenitors as they exit the cell cycle (Muranishi et al., 2011). These *Otx2*+ cells appear to give rise to five neuronal types: horizontal, amacrine and bipolar interneurons, and rod and cone photoreceptors (Baas et al., 2000; Brzezinski and Reh, 2015; Brzezinski et al., 2013; Emerson et al., 2013; Fossat et al., 2007; Nishida et al., 2003; Sato et al., 2007). *Otx2* is quickly lost in amacrines and horizontals, but is maintained by photoreceptors and bipolar cells into adulthood (Emerson et al., 2013; Koike et al., 2007; Nishida et al., 2003). Loss-of-function studies show that *Otx2* regulates fate choice in the retina. *Otx2* mutants lack photoreceptors and bipolar cells, but instead generate excess amacrine interneurons (Ghinia Tegla et al., 2020; Nishida et al., 2003; Sato et al., 2007; Yamamoto et al., 2020). Thus, the decision to express *Otx2* greatly influences the cell fate composition of the retina. Given that this decision occurs in the last cell cycle, the gene regulatory events upstream of *Otx2* occur in retinal progenitors. Progenitors express a wide variety of transcription factors, including several from the basic helix-loop-helix (bHLH) class that control fate decisions throughout the central nervous system (Hatakeyama and Kageyama, 2004; Hatakeyama et al., 2001; Wang and Harris, 2005). Which of these transcription factors, if any, controls *Otx2* activation during retinal development is unknown.

A major component of gene regulatory networks is noncoding *cis*-regulatory DNA sequences known as enhancers. Enhancers provide spatial and temporal specificity to gene expression programs throughout development (Benoist and Chambon, 1981; Gillies et al., 1983; Long et al., 2016). To reduce the number of potential *Otx2* regulators, we searched for enhancers that coincide with *Otx2* activation during retinal development. We previously used DNase I hypersensitivity site (DHS) sequencing to identify candidates within the mouse retina (Wilken et al., 2015). Three DHS sequence elements were able to drive reporter gene expression in OTX2+ retinal cells. Of note was the DHS-4 element. Compared with the other elements, DHS-4 expression was highest at postnatal day (P) 0 and became severely restricted by P7 (Wilken et al., 2015). Based on this pattern, we hypothesized that DHS-4 acts by transiently initiating *Otx2* expression as progenitors exit the cell cycle. By determining which sequences were necessary for DHS-4 expression in the retina, we reasoned that the repertoire of transcription factors that activate *Otx2* could be identified.

We tested the role of the DHS-4 enhancer by: (1) examining its expression pattern in retinal development; (2) dissecting its

[1]Department of Ophthalmology, University of Colorado Anschutz Medical Campus, Aurora, CO 80045, USA. [2]Department of Cell Biology, University of Oklahoma Health Sciences Center, Oklahoma City, OK 73104, USA.

*Author for correspondence (joseph.brzezinski@cuanschutz.edu)

M.L.K., 0000-0003-2441-5836; N.B.G., 0000-0002-1376-1541; K.U.P., 0000-0002-8254-5826; M.S., 0000-0001-5497-9283; E.O., 0000-0003-2314-5213; S.R.S., 0000-0002-9756-5336; J.A., 0000-0002-9122-1778; A.H., 0000-0003-1498-3012; K.L.J., 0000-0003-4572-3651; J.A.B., 0000-0001-5854-0315

Handling Editor: François Guillemot
Received 6 January 2021; Accepted 10 May 2021

Development (2021) 148, dev199399. doi:10.1242/dev.199399

necessary sequence components; (3) testing whether it was required for OTX2 activation; and (4) identifying its upstream regulators. Consistent with our prediction, DHS-4 was transiently expressed during retinal development and became active as progenitors exited the cell cycle. We showed that DHS-4 is necessary for OTX2 expression and that this enhancer requires several bHLH transcription factor-binding sites for its activity. Using single cell RNA-sequencing, we identified the progenitor bHLH transcription factors *Ascl1* and *Neurog2* as potential upstream regulators of DHS-4 and *Otx2*. Loss-of-function analysis of *Ascl1* and *Neurog2* using a CRISPR/Cas9 approach showed that targeting these genes simultaneously, but not singly, reduced OTX2 expression. Our findings suggest a mechanism whereby bHLH transcription factors act redundantly or in a compensatory fashion at the DHS-4 enhancer to activate *Otx2* expression as retinal progenitors exit the cell cycle. Interestingly, removing DHS-4 from the postnatal retina had only a modest effect on OTX2 expression. This suggests that there is also redundancy or compensation at the level of enhancer usage. Together, our findings show that the gene regulatory network that controls *Otx2* activation is remarkably flexible and resistant to perturbation. Such regulatory network robustness may be necessary to ensure that the retina forms a sufficient number of OTX2+ rods, cones and bipolar cells.

RESULTS

Identification of an early minimal enhancer of *Otx2*

Otx2 becomes activated in the terminal cell cycle during retinal development (Muranishi et al., 2011). We hypothesized that a single enhancer is required for *Otx2* activation. Based on its early and potentially transient activity in the developing retina, we focused on the enhancer sequence identified as DHS-4 (Wilken et al., 2015). DHS-4 is a 1489 bp highly conserved region located ∼50 kb downstream of the *Otx2* translational initiation codon within exon 3 (Fig. 1A). To examine the spatial and temporal expression pattern of DHS-4, we used a reporter assay in which the enhancer sequence was cloned adjacent to a minimal TATA promoter (Mills et al., 2017; Wilken et al., 2015). Together, these two elements drive expression of a nuclear-localized GFP cassette. To control for electroporation efficiency, we used a ubiquitously expressed EF1α nuclear mCherry (RFP) plasmid (Mills et al., 2017; Wilken et al.,

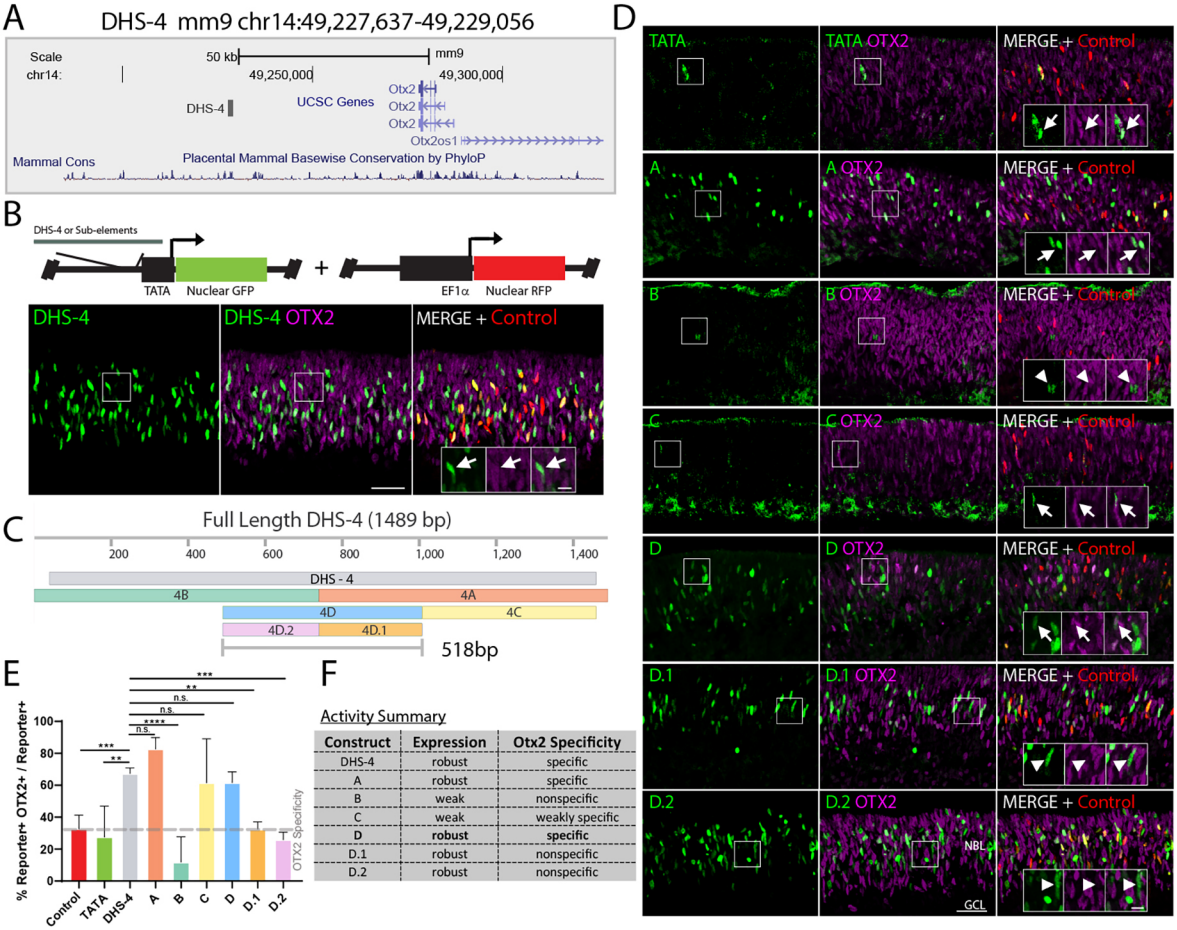

Fig. 1. DHS-4D is a minimal *Otx2* enhancer. (A) Mouse mm9 UCSC Genome Browser tracks displaying genomic coordinates of the DHS-4 sequence, *Otx2* coding variants and placental mammalian conservation. (B) Enhancer screening in retinal explants by electroporation at P0. Expression patterns of the DHS-4-TATA-GFP construct and ubiquitous RFP (mCherry) control in P0 retinas following 2 days of culture. Explants were stained for OTX2, GFP and RFP. Arrows mark OTX2+/GFP+ cells. (C) Dissection of parent DHS-4 sequence into sub-elements. (D) Expression patterns of DHS-4 sub-element constructs and RFP controls as described in B. Arrows mark GFP+/OTX2+ cells, arrowheads mark GFP+/OTX2− cells. (E) Quantification of DHS-4 parent and sub-element overlap with OTX2 expression compared with TATA-only and RFP co-electroporation controls. The dashed gray line represents the probability of an electroporated cell co-expressing OTX2. (F) Table summarizing the degree and specificity of sub-element expression. Data are mean±s.d.; n=3 explants per condition. **P<0.005, ***P<0.001, ****P<0.0001 (one-way ANOVA). n.s., not significant. Scale bars: 100 µm; 25 µm for insets. GCL, ganglion cell layer; NBL, neuroblastic layer.

Development (2021) 148, dev199399. doi:10.1242/dev.199399

2015). GFP and mCherry plasmids were co-electroporated into P0 mouse retinal explants and cultured for 2 days. Using immunohistochemistry, we observed numerous GFP+ cells that highly, yet incompletely, overlapped with OTX2 (Fig. 1B). This matched the previously observed DHS-4 pattern (Wilken et al., 2015).

We next investigated which sequences in the DHS-4 enhancer were crucial for its regulation. Given the relatively long (>1.4 kb) length of this sequence, we first sought to identify the smallest sub-element that recapitulated the DHS-4 expression pattern. To do this, we cloned sub-elements (Fig. 1C) of the parent DHS-4 sequence into the same TATA-GFP reporter backbone and electroporated P0 retinal explants. After 2 days, explants were stained for GFP, mCherry (RFP) and OTX2. Ubiquitous mCherry control plasmid electroporated cells co-expressed OTX2 32.6% of the time (Fig. 1D,E). Empty plasmid (TATA-only) controls showed similar co-expression with OTX2, but few GFP+ cells were seen (Fig. 1D,E). The DHS-4 parent construct had 67.4% overlap with OTX2 (Fig. 1B,E), significantly higher than TATA-only and ubiquitous mCherry controls (one-way ANOVA, $P<0.001$ and $P<0.0001$, respectively). Sub-elements DHS-4A and 4B bisected the 1489 bp region (Fig. 1C). Sub-element 4A had GFP reporter activity and maintained overlap with OTX2 expression that was similar to that in the DHS-4 parent, whereas sub-element 4B had weak nonspecific expression from only a few GFP+ cells (Fig. 1D,E).

We further dissected sub-element 4A and tested a sequence from the distal-most end, sub-element 4C (Fig. 1C). This highly overlapped with OTX2, but had weak reporter activity from only a few GFP+ cells (Fig. 1D,E). Next, we isolated the sequence of sub-element 4A that was not included in sub-element 4C and added adjacent sequence from 4B (Fig. 1C). This sub-element, designated 4D, displayed both robust expression and high overlap (61.6%) with OTX2, which was significantly higher than controls and indistinguishable from the DHS-4 parent (one-way ANOVA, $P<0.0001$ versus mCherry, $P<0.05$ versus TATA and $P=0.1797$ for DHS-4) (Fig. 1D,E). We then bisected the 4D sequence into D.1 and D.2 sub-elements (Fig. 1C). Both of these sub-elements were highly expressed, similar to sub-element 4D; however, intriguingly, they lost their specificity with OTX2, having only 32.6% and 25.9% overlap, respectively, and were indistinguishable from mCherry or TATA-only controls (one-way ANOVA, D.1 versus mCherry $P=0.9852$, D.1 versus TATA $P=0.5468$, D.2 versus mCherry $P=0.1035$, D.2 versus TATA $P=0.8598$) (Fig. 1C-E). Based on these findings, we considered 4D to represent the minimal enhancer sequence that recapitulated the expression pattern of the full-length DHS-4 sequence (Fig. 1F) (Wilken et al., 2015). The 518 bp DHS-4D sequence was used in downstream experiments.

DHS-4D transiently marks *Otx2*+ cells

The DHS-4 enhancer shows activity during embryonic and early postnatal retinal development, but never completely overlaps with OTX2 (Fig. 1) (Wilken et al., 2015). This raises the possibility that DHS-4 is made by proliferative cells as they activate *Otx2* and that the stable GFP signal persists in some postmitotic cells (e.g. amacrines and horizontals) that subsequently lose OTX2 expression. To further understand the cells marked by the DHS-4D reporter plasmid, we examined additional markers of early-born cell fates. We quantified the overlap of DHS-4D with AP2B (horizontals and amacrines), ONECUT1 (cones, horizontals and ganglion cells) and RXRG (cones and ganglion cells) (Fig. S1) (Bassett et al., 2012; Emerson et al., 2013; Roberts et al., 2005; Sapkota et al., 2014; Wu et al., 2012, 2013). We identified modest overlap with each of these markers, consistent with transient marking of cones, amacrines and horizontals by DHS-4D (Fig. S1). No DHS-4D expression was seen in the ganglion cell layer, suggesting that DHS-4D does not label ganglion cells. Given that *Otx2* expression is activated during the terminal cell cycle (Muranishi et al., 2011), we expected to see DHS-4D overlap with progenitor markers. P0 mouse retinas were electroporated, as before, with either a ubiquitously expressed control plasmid or the DHS-4D reporter and cultured for 2 days. Sections were stained with antibodies against Ki67, a marker associated with cell proliferation, and the overlap with GFP and mCherry was quantified (Fig. 2A). We found that DHS-4D overlapped with Ki67 30.8% of the time, consistent with the enhancer becoming active as progenitors upregulate OTX2 and exit the cell cycle (Fig. 2A). mCherry+ control cells were significantly less likely to co-express Ki67 (13%, unpaired *t*-test, $P<0.0001$) (Fig. 2A), further suggesting that DHS-4D is preferentially expressed during the terminal cell cycle. Next, we incorporated 5-ethynyl-2′-deoxyuridine (EdU) 30 min before collecting explants to mark S-phase cells. We saw few GFP+/EdU+ cells, suggesting that DHS-4D is primarily active following S-phase, similar to OTX2 (Fig. 2B) (Muranishi et al., 2011). There were no significant differences in EdU incorporation between GFP and mCherry control cells (Fig. 2B).

DHS-4 enhancer activity appeared to decline with age (Wilken et al., 2015). This suggests that this enhancer is only transiently expressed or marks a restricted cell population in the mature retina. To test this, we conducted *in vivo* retinal electroporations in newborn mice. We electroporated the DHS-4 and DHS-4D reporters and examined their expression patterns at P25. Neither the parent DHS-4 nor the DHS-4D sub-element displayed expression at P25 (Fig. S2A). To further track this loss of expression, we modified a version of our enhancer reporter plasmid to express both GFP and Cre recombinase. This plasmid was electroporated into newborn *ROSA-RFP* reporter mouse retinas (Madisen et al., 2010). In this lineage-tracing system, cells that have enhancer activity at any timepoint would permanently express RFP, whereas the cells currently expressing DHS-4D would also express GFP (Fig. S2B). Using this lineage-tracing strategy with DHS-4D, we found, as early as P7, that there were many RFP+ cells, but none was GFP+ (Fig. S2B). These RFP+ cells were primarily photoreceptors and bipolar cells (OTX2+), but we observed some amacrine cells and the occasional ganglion or Müller glial cell based upon marker co-expression, morphology and laminar position (Fig. S2C). This is consistent with *Otx2* (and DHS-4D) being expressed by cells that can adopt an amacrine fate in addition to photoreceptors and bipolar cells that maintain OTX2 expression. Given that the lineage system is sensitive, this pattern may also reflect some nonspecific Cre recombinase activity. Taken together, our data argue that the DHS-4D enhancer is expressed in a transient fashion as progenitors exit the cell cycle and is not maintained in mature OTX2+ photoreceptors or bipolar cells.

The DHS-4D enhancer is required for embryonic OTX2 expression

Given its spatial and temporal pattern, we hypothesized that DHS-4D directly regulates *Otx2* initiation during development. To test this, we used a CRISPR/Cas9 strategy to delete the DHS-4D sequence by nonhomologous end joining (Goodson et al., 2020a). We showed that this was effective at perturbing enhancers both *ex vivo* and *in vivo* (Goodson et al., 2020a). We acquired the PX458 plasmid, which drives both single guide (sg) RNA expression from

Development (2021) 148, dev199399. doi:10.1242/dev.199399

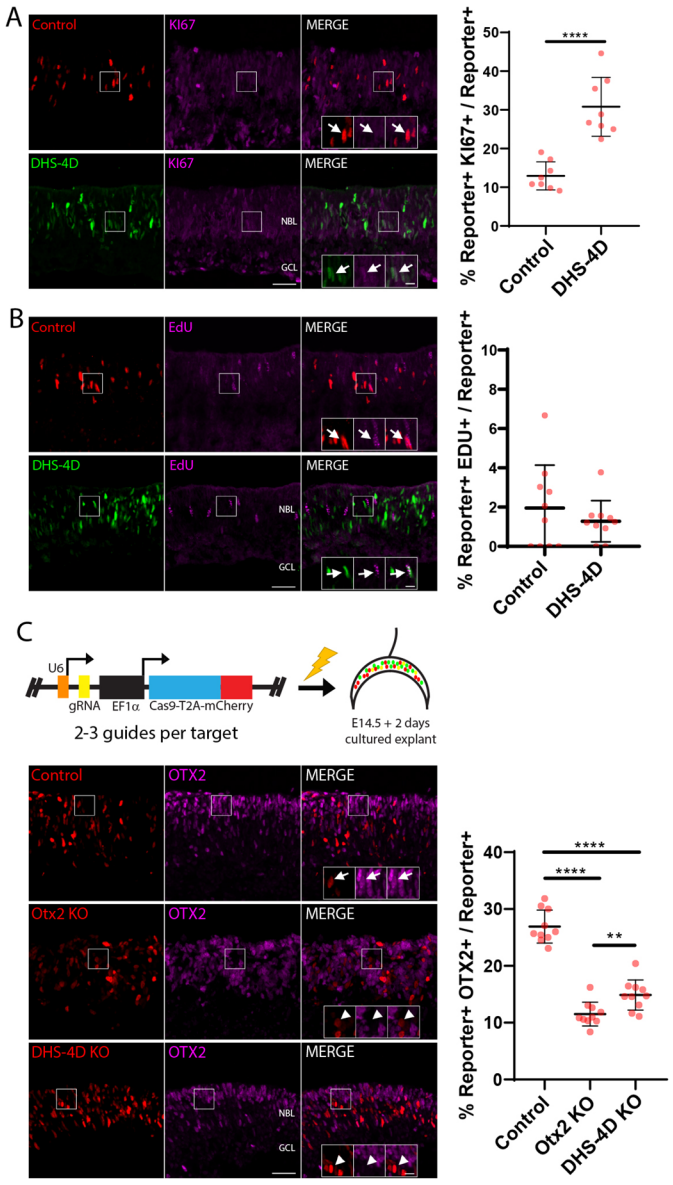

Fig. 2. DHS-4D marks proliferating cells and is required for embryonic OTX2 expression. (A,B) Histology and quantification of P0 explanted retinas electroporated with DHS-4D and control reporter constructs, cultured for 2 days and stained for Ki67 or EdU incorporation (30 min before harvest). Arrows mark double-labeled cells. Dots in the plots represent quantified images from three explants per condition. Bars show the mean±s.d. (C) Histology and quantification of E14.5 explanted retinas electroporated with CRISPR/Cas9 plasmids containing nontargeting control guides or guides against *Otx2* or DHS-4D (knockout; KO). Arrows mark double-labeled cells and arrowheads show single-labeled cells. Plots are as in A, with n=3 explants per condition. Significance determined by two-tailed unpaired *t*-test. **P<0.005, ****P<0.0001. Scale bars: 100 µm; 25 µm for insets. GCL, ganglion cell layer; NBL, neuroblastic layer.

a U6 promoter and Cas9 expression from a CMV promoter (Ran et al., 2013). We modified this plasmid to replace the CMV promoter with a ubiquitously expressed EF1α sequence that performs better in the retina (Goodson et al., 2020a; Ran et al., 2013; Semple-Rowland et al., 2010). In addition, we generated new plasmid variants with nuclear-localized versions of GFP and mCherry via fusion to histone H2B. This resulted in an all-in-one plasmid that expresses a targeting sgRNA, ubiquitous Cas9 and persistent nuclear reporters for cell tracking. Three guide plasmids were designed to remove the DHS-4D sequence (Fig. S3) and these were pooled and electroporated into retinal explants. Nontargeting guide plasmids were used as a negative control and guides targeting coding exons of *Otx2* were used as positive controls. Plasmids were electroporated into E14.5 explants and cultured for 2 days. Histological sections were stained for OTX2 and fluorescent protein reporter overlap was quantified. Nontargeting guide plasmid (GFP+) overlapped with OTX2 26.9% of the time (Fig. 2C). Positive-control *Otx2*-targeting guides reduced this to ∼11.5%, whereas targeting the DHS-4D enhancer reduced the overlap to 14.9% (Fig. 2C). Both *Otx2*-coding and DHS-4D targeting guides significantly reduced overlap with OTX2 compared with nontargeting controls (unpaired *t*-tests, P<0.0001 and P<0.0001, respectively) (Fig. 2C). Targeting either the DHS-4D- or *Otx2*-coding sequences was equally efficient at reducing OTX2 expression (Fig. 2C), suggesting that the DHS-4D enhancer is necessary for OTX2 expression in the embryonic retina.

DHS-4 sub-element D contains E-box motifs required for its expression

Given that the DHS-4D enhancer was necessary for embryonic OTX2 expression, we reasoned that its essential transcription factor-binding sites would predict the regulatory network that activates *Otx2*. A cursory examination of the DHS-4D sequences revealed several enhancer box (E-box) response elements (Fig. S4). The E-box-binding domain is characterized by the palindromic CANNTG motif sequence, which can act as a binding site for bHLH transcription factors (Murre et al., 1994). These transcription factors typically bind in a heterodimeric fashion to the E-box, facilitating transcription (Ellenberger et al., 1994; Henke et al., 2009). We identified a total of six canonical E-box sites within DHS-4D (Fig. 3A; Fig. S4).

To test the necessity of these E-boxes for DHS-4D expression, we systematically mutated the sites. To inactivate these sites with the least disruption of the overall DHS-4D sequence, we used a previously reported strategy in which the CANN′TG′ motif is mutated to CANN′AT′ (Fig. 3B). This was shown to prevent activity of bHLH factors because of a lack of DNA-binding specificity (Henke et al., 2009). We co-electroporated E-box mutated reporter constructs with ubiquitous mCherry control plasmids into E14.5 retinal explants and cultured them for 2 days (Fig. 3B). We first mutated single E-box sites, as numbered in Fig. 3A. Explants were stained for GFP, RFP and OTX2, as described above. We found that E-boxes 3, 4 and 6 were each essential for DHS-4 expression because these explants lacked GFP+ cells (Fig. 3C,D). In contrast, mutating E-boxes 1, 2 or 5 resulted in continued robust GFP expression and OTX2 overlap (Fig. 3C,D).

The six E-box sites were not evenly distributed in DHS-4D but formed two clusters (1-2 and 3-5) (Fig. 3A). To test whether there are interactions between the E-box sites, we mutated multiple E-boxes simultaneously and electroporated retinas as described above. This resulted in an additional ten mutant constructs (Fig. 3C). As expected, mutating all six E-box motifs to CANN′AT′ completely prevented enhancer activity (Fig. S5). Constructs that contained mutated E-boxes 3, 4 or 6 were always inactive, replicating the single mutagenesis experiments (Fig. S5). Surprisingly, a construct with the three nonessential sites mutated (1, 2 and 5) was also devoid of reporter activity (Fig. 3C; Fig. S5). This indicated that the essential E-box sites (3, 4 and 6) were not sufficient to drive enhancer expression, highlighting a cooperative requirement beyond the essential sites.

Development (2021) 148, dev199399. doi:10.1242/dev.199399

Single cell RNA-sequencing reveals bHLH transcription factors upregulated along *Otx2* developmental trajectories

The factors that regulate DHS-4D expression are genetically upstream of *Otx2*. Our mutagenesis experiments argue that enhancer and *Otx2* expression is regulated by bHLH transcription factors. We previously showed that disruption of Notch signaling through small molecule γ-secretase inhibitors in murine E14.5 retinal explants resulted in an increase in *Otx2* and cone photoreceptor formation (Kaufman et al., 2019). Transcriptionally profiling these explants over time revealed that expression of several bHLH transcription factors, including Ascl1, Neurog2 and Olig2, preceded the onset of *Otx2* expression (Kaufman et al., 2019). To improve our temporal resolution and bypass potential issues from perturbed development, we used a single cell RNA-sequencing approach to identify which bHLH genes are expressed immediately upstream of *Otx2*.

To gain temporal information upstream of *Otx2* activation, we profiled progenitors as they became OTX2+ cells. E14.5 mouse retinas were electroporated with both a DHS-4D-GFP reporter and a ubiquitous mCherry control plasmid (Fig. 4A). Retinas were cultured for up to 2 days and then subjected to fluorescence-activated cell sorting (FACS). The DHS-4D-GFP+ population represented cells that had activated *Otx2*. Cells that only expressed mCherry represented *Otx2*− cells, such as progenitors and ganglion cells. To obtain a representation of developing cells along a progenitor to *Otx2*+ state, we mixed GFP+ (±mCherry) and mCherry-only cells to be 40% and 60% of the total, respectively (Fig. 4A). These cells were subjected to 10X Genomics Chromium single cell capture, labeling and high-throughput sequencing (Fig. 4A). We captured 1843 cells and our read depth was ∼250K per cell, allowing us to map potentially under-represented RNAs. Following quality control, we identified 13 clusters by Uniform Manifold Approximation and Projection (UMAP) dimension reduction using Leiden-based clustering in the Scanpy Python package (Fig. 4B) (McInnes et al., 2018; Wolf et al., 2018). Comparing DHS-4D-GFP and *Otx2* mRNA expression on the UMAP representation showed that the *GFP* signal marks a subset of the *Otx2*+ cells, consistent with the transient expression pattern of the enhancer (Fig. 4B).

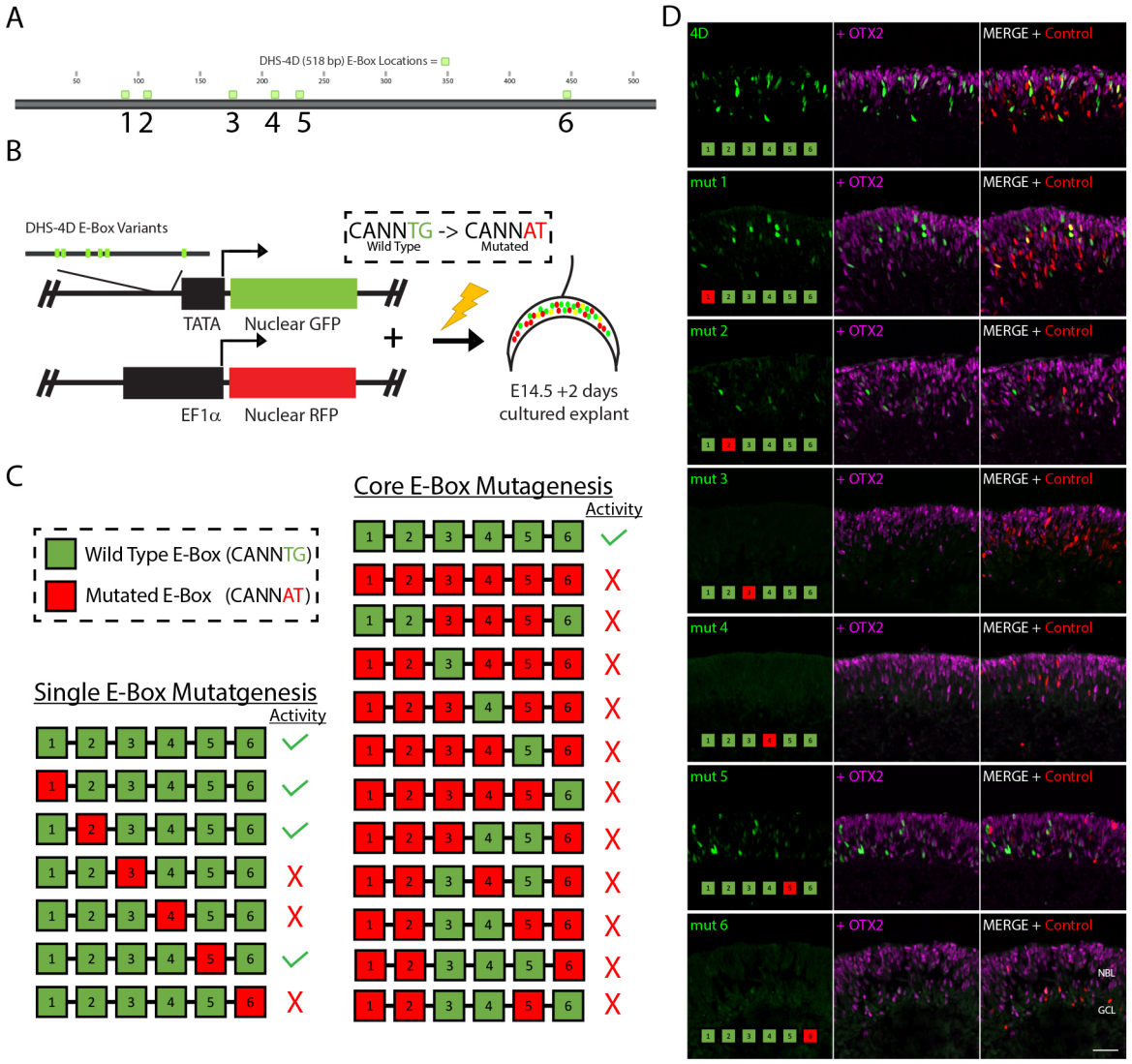

Fig. 3. DHS-4D requires E-box motifs for its expression. (A) Location of six CANNTG E-Box motifs within the DHS-4D sequence. (B) Design of the electroporation screen of nonfunctional mutant (CANNTG->CANNAT) E-boxes. (C) Summary of the activity displayed by each mutant construct compared with the parent DHS-4D sequence. The red X marks indicate constructs that lack either activity or specificity. (D) Representative histology for multiple constructs showing the control DHS-4D expression pattern versus single E-box mutants. Scale bar: 100 µm. GCL, ganglion cell layer; NBL, neuroblastic layer.

Development (2021) 148, dev199399. doi:10.1242/dev.199399

We next performed cluster analysis and used known markers to classify progenitors (*Fgf15*, *Vsx2*, *Sox2*, *Pax6*), photoreceptors (*Otx2*, *Crx*, *Prdm1*, *Rxrg*, *Thrb*, *Pdc*, *Gnat2*, *Gngt2*, *Nrl*), amacrines/horizontals (*Ptf1a*, *Prdm13*, *Tfap2a*, *Tfap2b*, *Onecut1*, *Onecut2*, *Lhx1*, *Prox1*, *Ebf1*) and ganglion cells (*Isl1*, *Rbpms*, *Pou4f1*, *Pou4f2*) manually (Fig. 4C). These cell-type annotations were then mapped back onto the UMAP cluster number they most represented (Fig. S6). Consistent with their embryonic age, the clusters represent progenitors (0, 1, 2, 5, 6, 11 and 13), cone photoreceptors (clusters 4 and 12), amacrines and horizontals (clusters 7 and 10) and ganglion cells (cluster 8) (Fig. S6). Clusters 3 and 9 did not fit definitively into a specific group, but were likely progenitors transitioning into a neuronal state (Fig. 4C) (Clark et al., 2019). Comparing these progenitor clusters with the previously classified populations described (Clark et al., 2019), we found that they fell into two broad groups. Clusters 0, 1 and 5 likely represent early/intermediate progenitors because of their relatively high levels of *Fgf15*, *Vsx2* and *Sox9*. Clusters 2, 6 and 11 can be classified as neurogenic or late neurogenic progenitors based on their expression of *Otx2*, *Ascl1*, *Neurog2* and *Olig2* (Fig. S6). Differences in the stage of the cell cycle likely underlie the relatively large number of progenitor clusters we identified (Fig. S6). *DHS-4D-GFP* expression was most highly detectable in clusters 2, 3, 6 and 11 (Fig. 4C). This expression pattern overlapped with *Otx2* and the clusters representing progenitors and other cells transitioning into cones, amacrines and horizontal interneurons (Fig. 4C).

Trajectory analysis to identify gene expression events along developmental pathways was performed using the diffusion pseudotime function in the Scanpy Python package (Haghverdi et al., 2016). Cells were aligned according to their pseudotime score and plotted in ForceAtlas2 component space, with the original Leiden clusters represented (Jacomy et al., 2014) (Fig. 4D). To identify factors upstream of *Otx2*, we isolated a pseudotime pathway that ended in the cone photoreceptor cluster (12), a state in which *Otx2* becomes permanently maintained (Fig. 4D) (Koike et al., 2007; Nishida et al., 2003). This pathway includes clusters 2, 3, 6 and 11, which have the highest-detectable levels of *DHS-4D-GFP* (Fig. 4C). Expression of candidate bHLH factors and known

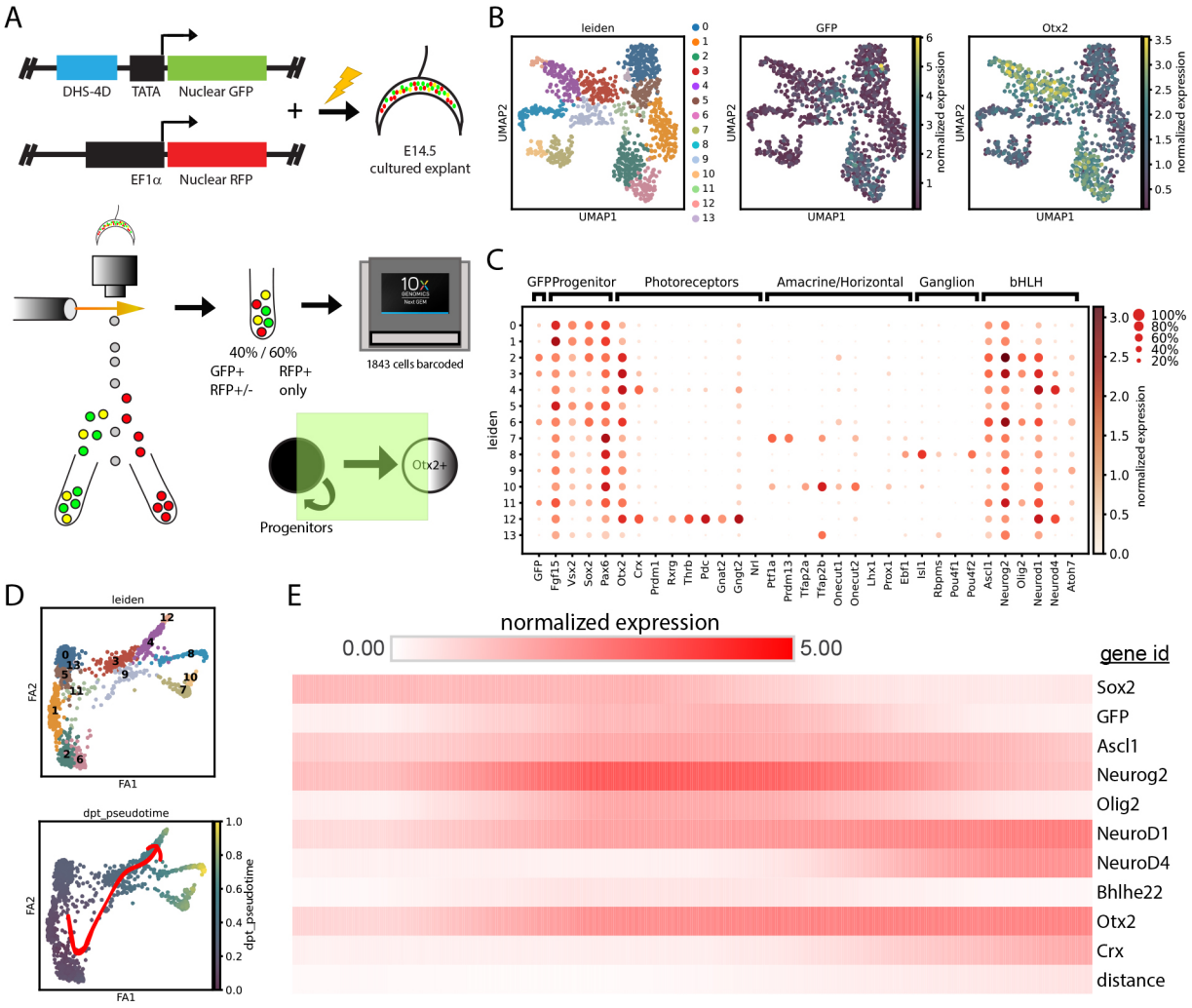

Fig. 4. Single cell RNA-sequencing reveals bHLH transcription factors upregulated along *Otx2*+ developmental trajectories. (A) Experimental design of single cell RNA-sequencing to enrich for DHS-4D+ cells and identify candidate activating transcription factors. (B) Plots showing UMAP clustering of cells and normalized expression of *GFP* and *Otx2*. (C) Marker genes for each cluster designating the likely cell types. The expression of selected bHLH transcription factor genes is shown. (D) Force Atlas 2 projection of Leiden clusters (numbers as given in C). The bottom plot shows pseudotime overlaid onto the Forced Atlas projection. The solid-red line indicates the OTX2+ trajectory analyzed in E. (E) Pseudotime trajectory showing normalized expression of selected candidate regulatory factors along the *Otx2*+ trajectory. *Crx* is included as a downstream target of *Otx2*.

Development (2021) 148, dev199399. doi:10.1242/dev.199399

markers was plotted along this trajectory (Fig. 4E). Recapitulating the pattern seen from reporter and lineage-tracing experiments (Figs 1, 2; Figs S1, S2), *DHS-4D-GFP* tracked a subset of cells in a transitory state overlapping both *Sox2*+ progenitors and *Otx2*+/*Crx*+ photoreceptors (Fig. 4E). Analysis of transcription factors overlapping in pseudotime with the *DHS-4D-GFP*+ cells revealed several bHLH candidates, including *Neurod1*, *Bhlhe22*, *Ascl1*, *Neurog2* and *Olig2* (Fig. 4E). These candidates were similar to those we observed upon inhibiting Notch signaling in E14.5 explants (Kaufman et al., 2019). The expression of the candidate bHLH factors over pseudotime was not equivalent (Fig. 4E). Some factors showed robust transient expression (*Ascl1*, *Olig2* and *Neurog2*), others appeared to be upregulated late (*Neurod1* and *Neurod4*) and *Bhlhe22* had only modest transient upregulation (Fig. 4E). Based on their co-expression, timing of upregulation and their transient nature, we considered *Ascl1*, *Neurog2* and *Olig2* to be the most-likely regulators of DHS-4D and *Otx2* activation.

Combinatorial loss of *Ascl1* and *Neurog2* inhibits OTX2 expression

Results from our mutagenesis and single cell RNA-sequencing experiments supported the hypothesis that bHLH transcription factors made by progenitors bind the E-boxes of the DHS-4D enhancer to activate *Otx2* expression. This was also supported by strong JASPAR binding predictions at these sites (Fig. S7). Furthermore, we predicted that removing *Ascl1*, *Neurog2* and/or *Olig2* would prevent OTX2 expression, similar to CRISPR/Cas9 targeting of the DHS-4D enhancer sequence (Fig. 2C). To test this, we used our CRISPR/Cas9 approach to target the bHLH transcription factors. Guides were made to target early coding exons of each bHLH gene. These were electroporated into E14.5 explants and the retinas were screened after 2 days of culture (Fig. 5A). We first examined changes in bHLH factor expression compared with nontargeting guide controls. We found that targeting *Ascl1*, *Olig2* and *Neurog2* resulted in strong reductions in their protein expression compared with nontargeting control (unpaired *t*-tests, $P<0.0001$, $P<0.0001$ and $P<0.0001$, respectively) (Figs S8, S9). Similar to targeting *Otx2* or DHS-4D (Fig. 2C), this did not reach 100% efficiency for *Ascl1*, *Olig2* or *Neurog2*.

We then tested whether targeting these bHLH factors affected OTX2 expression. Singly targeting *Ascl1*, *Neurog2* or *Olig2* did not have a significant effect on OTX2 expression compared with nontargeting guides or previous *Otx2* targeting (unpaired *t*-tests, $P=0.853$, $P=0.164$ and $P=0.415$ compared with nontargeting guides, respectively) (Fig. 2C, Fig. 5A; Fig. S9). This was consistent with the mild phenotypes previously reported from single mutations of these genes (Akagi et al., 2004; Brzezinski et al., 2011; Hafler et al., 2012; Hufnagel et al., 2010; Tomita et al., 1996). The DHS-4D element contains multiple E-boxes, none of which was sufficient on its own for enhancer activity (Fig. 3). Our single cell analysis showed that there were several bHLH factors expressed at the right time and place to regulate DHS-4D (Fig. 4). Thus, we reasoned that multiple bHLH factors can activate DHS-4D and *Otx2* expression in a redundant or compensatory fashion. To test this hypothesis, we used additional reporter fluorescent proteins to visualize combinational effects of multiplexed gene targeting (Fig. 5A). These were then combined into a single pooled mixture and electroporated into E14.5 explants, an approach we previously showed to be highly efficient (Goodson et al., 2020a). The percentage of electroporated cells that co-expressed OTX2 was significantly reduced in *Ascl1/Neurog2* double-targeted cells compared with nontargeting and single-targeted controls ($P<0.0001$) (Fig. 5B). This reduction was similar in magnitude to *Otx2* and DHS-4D targeting (Fig. 2). We also targeted *Ascl1*, *Neurog2* and *Olig2* simultaneously, but we did not observe an additive effect on OTX2 expression (Fig. S9). This was unlikely due to dilution effects, because the triple-targeting condition was equally effective at reducing OLIG2 expression as singly targeting *Olig2* (Fig. S9). To assess whether bHLH removal perturbed the cell cycle and indirectly influenced OTX2 expression, we quantified the double *Ascl1*/*Neurog2*-targeted electroporations with Ki67 and EdU labeling. No differences were found between controls and knockouts (unpaired *t*-test, Ki67 $P=0.3577$ and EdU $P=0.9858$) (Fig. S10). Next, we targeted *Ascl1* and *Neurog2* at the P0 timepoint in explants along with negative control and *Otx2*-targeting guides, and quantified retinas after 3 days of culture (Fig. 5C). Whereas both *Otx2* and *Ascl1/Neurog2* targeting significantly reduced OTX2 co-expression (unpaired *t*-tests, $P<0.0001$ and $P<0.0001$, respectively), double bHLH targeting only reduced overlap to 36.1% compared with 12.6% in direct *Otx2* targeting (unpaired *t*-test, $P=0.0001$) (Fig. 5D).

Together, our findings suggest that *Ascl1* and *Neurog2* regulate *Otx2* expression via the DHS-4D enhancer. Given that only targeting *Ascl1* and *Neurog2* simultaneously affected OTX2, our results highlight the possibility that compensatory or redundant mechanisms are at play. Interestingly, these effects were diminished at later developmental timepoints, raising the possibility that other enhancers or transcription factors can activate *Otx2* postnatally.

Targeting DHS-4D in newborn mice partially affects OTX2 expression

Perturbing the DHS-4D sequence with CRISPR/Cas9 severely reduced OTX2 expression in E14.5 explants. We reasoned that, if the DHS-4D enhancer was essential for *Otx2* activation throughout retinal development, then targeting DHS-4D at P0 should block OTX2 expression and change fate choice in the retina. Alternatively, if another enhancer can take the place of DHS-4D later during development, targeting DHS-4D would have a modest effect on OTX2. To discriminate between these possibilities, we conducted *in vivo* electroporation with our DHS-4D-targeting CRISPR/Cas9 plasmids in newborn mice and harvested eyes at P7 (Fig. 6A). As before (Fig. 2C), we electroporated guides against DHS-4D and *Otx2*, or used nontargeting guides as a negative control. The retinas from P7 eyes were immunostained for their fluorescent reporter and OTX2 (Fig. 6B). As with embryonic timepoints, *Otx2*-targeted cells co-expressed OTX2 at approximately one-third the rate of nontargeting guide controls (unpaired *t*-test, $P<0.0001$) (Fig. 6C). Many of the *Otx2*-targeted cells lacked OTX2 co-expression and resided in the inner portion of the inner nuclear layer, consistent with an amacrine fate. This fate change is consistent with the phenotype of conditional *Otx2*-mutant mice and targeted knockouts (Ghinia Tegla et al., 2020; Nishida et al., 2003; Sato et al., 2007; Yamamoto et al., 2020). Compared with controls, fewer DHS-4D-targeted cells co-expressed OTX2 (unpaired *t*-test, $P<0.0001$) and more electroporated cells were observed in the amacrine area of the inner retina (Fig. 6B,C). Nonetheless, targeting DHS-4D had a significantly weaker effect on OTX2 expression than did targeting the *Otx2*-coding region (one-way ANOVA, $P<0.0001$) (Fig. 6C). This suggests that another enhancer can contribute to *Otx2* activation when DHS-4D is perturbed in the postnatal retina. A similar diminished effect on OTX2 expression was seen when both *Ascl1* and *Neurog2* were targeted in P0 explants cultured for 3 days

Development (2021) 148, dev199399. doi:10.1242/dev.199399

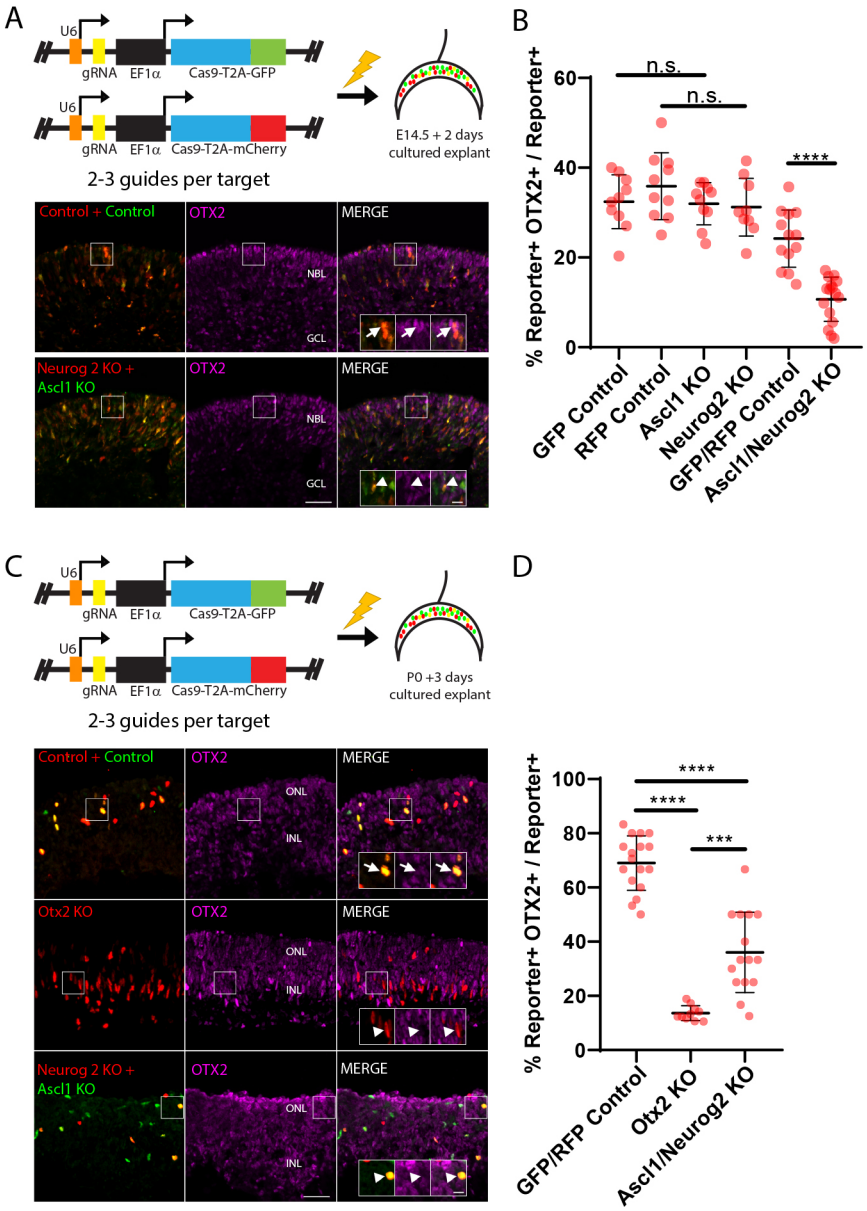

Fig. 5. Combinatorial loss of *Ascl1* and *Neurog2* is required to inhibit OTX2 expression.
(A) Experimental design and representative histological images for combinatorial CRISPR/Cas9 targeting of *Ascl1* and *Neurog2* (knockout; KO) in E14.5 explants cultured for 2 days. Arrows mark reporter+/OTX2+ cells, arrowheads show reporter+/OTX2− cells. (B) Quantification of OTX2 overlap with electroporated cells. Dots represent quantified images from 3-6 explants per condition. Bars show the mean±s.d. (C) Experimental design to target *Ascl1*, *Neurog2* or *Otx2* (KO) in P0 explant retinas cultured for 3 days. Representative histology is as described in A. (D) Quantification of OTX2 overlap as in B, with n=4 explants per condition. ***P<0.001, ****P<0.0001 (two-tailed unpaired t-test). n.s., not significant. Scale bars: 100 µm; 25 µm for insets. GCL, ganglion cell layer; INL, inner nuclear layer; NBL, neuroblastic layer; ONL, outer nuclear layer.

(Fig. 5C). Correspondingly, simultaneously targeting *Ascl1* and *Neurog2* at P0 had no effect on OTX2 co-expression at P7 (Fig. 6B,C). Taken together, our findings suggest that additional enhancers and transcription factors activate or sustain OTX2 expression in the postnatal retina.

DISCUSSION

Retinal development is governed by complex gene regulatory networks that are only partially understood. To dissect the *Otx2* gene regulatory network, we characterized the function of a minimal enhancer sequence, termed DHS-4D, and demonstrated that it recapitulated the pattern of *Otx2* expression initiation during development. This enhancer was necessary for OTX2 expression and its activity depended on E-box bHLH transcription factor-binding sites. Correspondingly, perturbing the bHLH factors *Ascl1* and *Neurog2* simultaneously prevented OTX2 expression. Our data suggest that bHLH factors made by progenitors during their terminal cell cycle activate the DHS-4D enhancer to initiate *Otx2* expression. Initiating *Otx2* expression appears to have redundant and/or compensatory features, both in terms of which transcription factors are involved and the *cis*-regulatory enhancers used. The gene regulatory network controlling *Otx2* is complex and flexible. This may make gene expression more robust to ensure that normal fate decisions occur during retinal development.

DHS-4 initiates *Otx2* expression during retinal development

During retinal neurogenesis, *Otx2* is activated by a large subset of progenitors in their terminal division (Fig. 7) (Muranishi et al., 2011). Most of these cells will maintain *Otx2* expression and become photoreceptors and bipolar cells (Fig. 7B). A smaller fraction will lose *Otx2* expression and adopt amacrine and horizontal fates (Fig. 7B). The DHS-4D enhancer was enriched in OTX2+ cells, but showed transient activity in the retina (Fig. 7A). At embryonic timepoints, the enhancer marked OTX2+ cells (e.g. cones), progenitors, amacrines and horizontal cells (Fig. S1). Our postnatal DHS-4D lineage tracing showed that this enhancer drives transient expression, but contributes to photoreceptor, bipolar and amacrine cell fates (Fig. S2). This transient expression

Development (2021) 148, dev199399. doi:10.1242/dev.199399

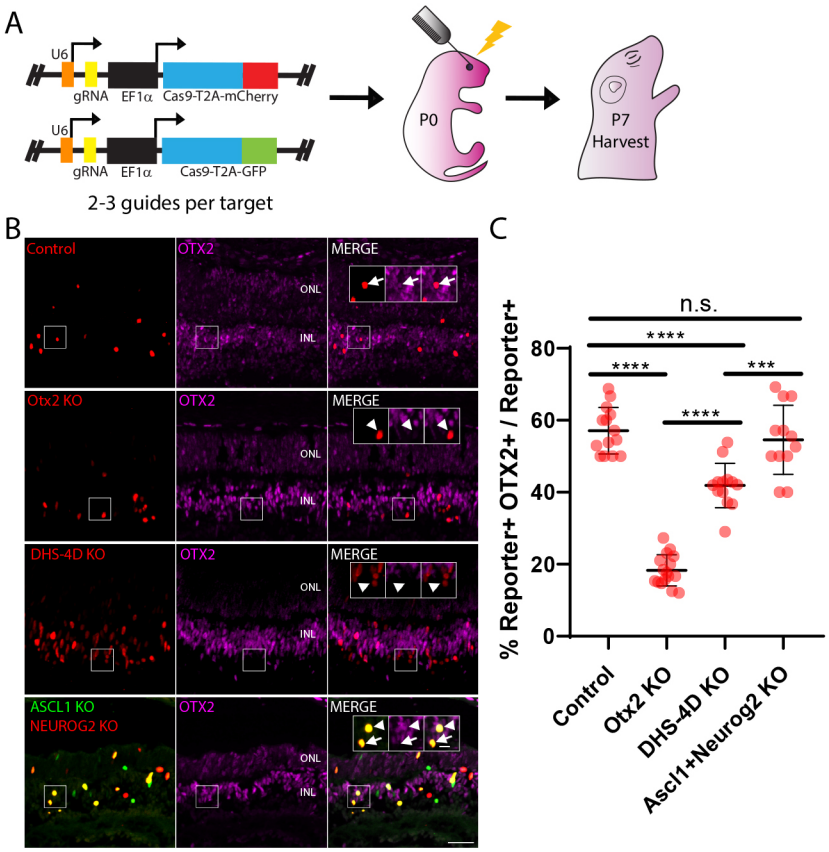

Fig. 6. Postnatal targeting of DHS-4D has a modest effect on OTX2 expression. (A) Experimental design to target DHS-4D or *Otx2* (knockout; KO) in live P0 mouse retinas harvested 1 week after electroporation. (B) Representative histology and quantification from control, *Otx2*, DHS-4D and *Ascl1*/*Neurog2*-targeting conditions. Arrows mark double-labeled cells, arrowheads mark reporter+/OTX2− cells. (C) Dots represent quantified images from 3-4 mice per condition. Bars show mean±s.d. ***P<0.001, ****P<0.0001 (one-way ANOVA). n.s., not significant. Scale bars: 100 µm; 25 µm for insets. INL, inner nuclear layer; ONL, outer nuclear layer.

was also seen in our single cell RNA-sequencing analysis, in which DHS-4D-driven *GFP* mRNA was expressed by progenitors as they activated *Otx2* and was quickly downregulated as cells became photoreceptors (Fig. 4). Our findings suggest that the DHS-4D enhancer acts by initiating *Otx2* expression as progenitors exit the cell cycle (Fig. 7B). This initiator role was supported by the requirement for DHS-4D during early development and by the necessity for *Ascl1* and *Neurog2* for OTX2 expression. These two bHLH factors are likely to act only as *Otx2* initiators because their expression tapers off sharply as progenitors become postmitotic cells (Fig. 4C) (Brzezinski et al., 2011; Hufnagel et al., 2010; Maurer et al., 2018).

DHS-4D is regulated by bHLH and other transcription factors

We reduced the DHS-4 enhancer down to a 518 bp DHS-4D sequence, which retained the spatial and temporal features of the parent element. Conspicuous within the DHS-4D sequence were six conserved E-box motifs. E-boxes 3, 4 and 6 were required for DHS-4D activity, arguing that bHLH transcription factors are necessary for enhancer and *Otx2* expression. CRISPR/Cas9 targeting of *Ascl1* and *Neurog2* reduced OTX2 expression, strongly implying that these two factors bind one or more E-boxes within the DHS-4D enhancer. This is supported by recently published ASCL1 chromatin immunoprecipitation (ChIP) sequencing data from P0 mouse retinas, which shows an ASCL1 binding peak within DHS-4D (Fig. S11) (Jorstad et al., 2020). Lack of detailed resolution limited the identification of which particular E-box was bound, but the peak was strongest around E-boxes 3, 4 and 5. Similar data for NEUROG2 were not available and our attempts at ChIP were unsuccessful. Thus, we were unable to determine whether NEUROG2 directly regulates DHS-4D under normal circumstances. However, DHS-4D-GFP expression substantially overlapped with ASCL1 (53.64%) and NEUROG2 (48.57%) embryonically (Fig. S12).

Although bHLH transcription factors regulate DHS-4D, other factors are likely involved in establishing its spatial and temporal pattern. Dividing DHS-4D into sub-elements (D.1 and D.2) resulted in constructs that lacked spatial specificity. This suggests that the spatial features of expression depend on other binding sites located within both the D.1 and D.2 halves of DHS-4D. One possibility is that the necessary E-box sites in each half synergize to drive the correct spatial activity. Alternatively, non-E-box sites may be required to establish specificity. This possibility is supported by recent work from Chan and colleagues, in which several sequences were screened for *Otx2* enhancer activity (Chan et al., 2020). They identified a 1.5 kb region, termed O9, which fully encompasses DHS-4D (Fig. S13) (Chan et al., 2020). The O9 element had transient activity in the developing retina, similar to DHS-4D. A 116 bp sub-element (O9-12) fully contained within the DHS-4D region also had retinal expression, although it was unclear whether it retained specificity with OTX2. Chan and colleagues showed that the O9-12 sub-element required a *Sox2*-binding site for retinal activity and that reducing *Sox2* expression with short hairpin (sh)RNA reduced the O9 parent enhancer activity (Chan et al., 2020). These data suggest that SOX2, made by progenitors, contributes to *Otx2* initiation via regulation of the DHS-4D enhancer. There are other conserved sequences and predicted binding sites throughout the enhancer, raising the possibility that additional transcription factors are essential for DHS-4D expression. It is likely that the combination of SOX2, bHLH and other transcription factors controls the spatial and temporal specificity of DHS-4D expression.

Development (2021) 148, dev199399. doi:10.1242/dev.199399

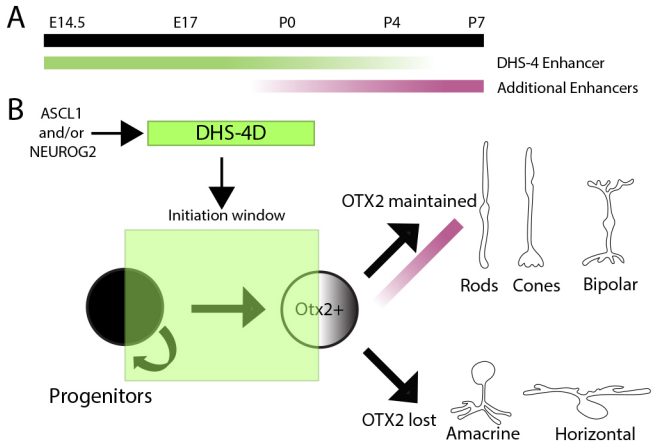

Fig. 7. Model of *Otx2* initiation and maintenance. (A) Separate enhancers are used to initiate and maintain *Otx2* expression in the retina. The DHS-4 enhancer is expressed as cells activate *Otx2*. Its expression is transient and seen only when progenitors are adopting neuronal fates. Additional unknown enhancers are responsible for *Otx2* expression after fate choices have been made. (B) ASCL1 and/or NEUROG2 are normally required to activate DHS-4D and initiate *Otx2* expression. OTX2 maintenance in photoreceptors and bipolar cells requires additional enhancers. Cells that adopt amacrine and horizontal fates do not maintain *Otx2* expression.

Redundant and compensatory mechanisms in the regulation of *Otx2*

We observed that the initiation of *Otx2* expression during retinal development had redundant or compensatory features. This occurred with transcriptional regulation and at the level of enhancer usage. Although CRISPR/Cas9 targeting of DHS-4D at embryonic times blocked OTX2 expression similarly to targeting its coding region, this was not the case in the postnatal retina. Late targeting resulted in only a partial loss of OTX2 expression. This closely paralleled targeting *Ascl1* and *Neurog2* postnatally, which only moderately reduced OTX2 expression. The concordance of these results suggests that another enhancer is partially redundant with DHS-4D or can incompletely compensate for its loss. In principle, the regulation of such an *Otx2* enhancer could be bHLH dependent. If so, the enhancer activity would not require *Ascl1* or *Neurog2*. It is unclear why this redundancy and compensation are apparent only in the postnatal retina. This effect could be due to changes in accessible chromatin flanking *Otx2*, leading to the addition/removal of enhancer sites, or in the complement of transcription factors expressed by progenitors over time. Another possibility is that, as the cell cycle length increases over development (Alexiades and Cepko, 1996), there is progressively more time for alternative pathways to compensate for the loss of the DHS-4D enhancer. The use of DHS-4D-knockout mice will help determine additional mechanisms of activating *Otx2* expression in the postnatal retina.

The loss of *Ascl1* and *Neurog2* in combination, but not alone, resulted in reduced OTX2 expression during embryogenesis. This further suggests that redundant or compensatory mechanisms are used to regulate DHS-4D and *Otx2* expression. Such mechanisms are consistent with the mild phenotypes seen in single-gene knockout experiments. Loss of *Neurog2* moderately affects ganglion cell differentiation and modestly alters OTX2+ cell populations (Hufnagel et al., 2010; Kowalchuk et al., 2018), whereas loss of *Ascl1* results in a modest depletion of progenitors and corresponding reductions in late-born cell types (Brzezinski et al., 2011; Nelson et al., 2009; Tomita et al., 1996). There are situations in which bHLH factors can compensate for each other to varying degrees. For example, *Neurod1* knock-in to the *Atoh7* locus was able to partially rescue the retinal ganglion genesis deficit that occurs in *Atoh7* null mice (Mao et al., 2008). In contrast, inserting *Ascl1* into the *Atoh7* locus did not rescue ganglion cell genesis (Hufnagel et al., 2010). Inserting *Neurog2* into the *Ascl1* locus can partially rescue some of the *Ascl1* mutant phenotypes in the developing brain (Parras et al., 2002). Other *Ascl1* and *Neurog2* mutagenesis experiments suggest a model in which specific bHLH factors are required in narrow temporal windows such that, when mutants delayed development, progression could be compensated for by a different bHLH factor expressed during the next developmental window (Hufnagel et al., 2010; Kowalchuk et al., 2018; Maurer et al., 2018; Pattyn et al., 2006). Indeed, delayed retinal development is a feature of both *Ascl1* and *Neurog2* mutants (Brown et al., 1998; Tomita et al., 1996). Lastly, mutating either *Ascl1* or *Neurog2* can result in the upregulation of the other factor in the developing retina (Akagi et al., 2004; Hufnagel et al., 2010; Kowalchuk et al., 2018). Together, these examples suggest that *Ascl1* or *Neurog2* can directly compensate for each other to activate *Otx2* expression.

It is also possible that *Ascl1* and *Neurog2* act in a redundant fashion during retinal development. Unlike some other areas of the developing nervous system, *Ascl1*, *Olig2* and *Neurog2* can be co-expressed within retinal progenitor cells (Fig. 4C) (Brzezinski et al., 2011; Hufnagel et al., 2010; Kaufman et al., 2019). Given their colocalization within retinal progenitor cells, redundancy could be enabled by the mere availability of each of these bHLH factors at the same time. In addition, although we observed that E-boxes 3, 4 and 6 were required for DHS-4D enhancer activity, these three sites were not sufficient to drive expression. This argues that bHLH factors bound at E-boxes 3, 4 and 6 interact with bHLH factors bound to sites 1, 2 and/or 5 to activate enhancer activity. This could reflect the requirement for a diverse set of bHLH transcription factors to be bound over multiple sites of an enhancer. This type of redundancy model was recently examined in embryonic stem cells, in which it was shown that a diverse assortment of transcription factors could drive enhancer expression far better than any single factor or binding site (Singh et al., 2021). The mutagenesis of multiple E-boxes may have limited the variety of bHLH factors that can occupy these sites, preventing the robust expression of DHS-4D. Similarly, it is possible that a threshold amount of bHLH factor binding at DHS-4D is sufficient to drive expression nonspecifically. In this model, single knockouts would not be sufficient to reduce the levels of bHLH factors below a threshold that generates a phenotype. By removing multiple bHLHs simultaneously (i.e. *Ascl1*/*Neurog2*), the overall amount of bHLH proteins may be reduced enough to cause a phenotype. This type of nonspecific threshold model is supported by reports that have shown a dose-dependent requirement of bHLHs to regulate or activate downstream function (Brown et al., 1998; Kataoka et al., 2000). Nonetheless, triple targeting of *Ascl1*, *Neurog2* and *Olig2* did not have a more-severe phenotype than double-targeting conditions. Thus, bHLH transcription factors may play more specifically defined roles in regulating *Otx2* expression.

Our findings cannot distinguish whether *Ascl1* and *Neurog2* act redundantly or compensate for each other during retinal development. Although ChIP-seq data show that ASCL1 binds DHS-4D (Jorstad et al., 2020), it is unclear whether NEUROG2 binds under normal conditions or only upon the loss of *Ascl1*. The former outcome would support a model of redundancy in which either bHLH factor could activate *Otx2*, whereas the latter result would argue that *Neurog2* directly compensates for the absence of *Ascl1*. It is also possible that both mechanisms are at play, but at different stages of development. ASCL1 and

Development (2021) 148, dev199399. doi:10.1242/dev.199399

NEUROG2 ChIP experiments at multiple stages of retinal development will help discriminate between compensatory and redundant mechanisms.

Regardless of whether *Ascl1* and *Neurog2* act in a redundant or a compensatory fashion, we were initially surprised that simultaneously targeting these factors blocked OTX2 expression in the embryonic retina. This was because *Ascl1/Neurog2/Neurod4* triple-mutant retinal explants cultured for 2 weeks form a laminated retina that contains photoreceptors (Akagi et al., 2004). Given that targeting *Ascl1* and *Neurog2* at birth had modest effects on OTX2, it is possible that only the early-born OTX2+ cells (cones and a small fraction of rods) are affected in double mutants. Cones were not specifically assayed in the triple-knockout retinas and could be severely reduced because such a deficiency could easily be masked by the formation of more-numerous late-born rod photoreceptors (Akagi et al., 2004). Another possibility is that combined loss of *Ascl1* and *Neurog2* results in delayed formation of OTX2+ neurons, a phenotype seen with ganglion and late-born OTX2+ cells in *Neurog2* mutants (Hufnagel et al., 2010; Kowalchuk et al., 2018; Maurer et al., 2018). Assaying the timing and extent of rod and cone photoreceptor genesis in *Ascl1/Neurog2* double-targeted cells would distinguish between these mechanisms.

Other enhancers are required for the maintenance of OTX2 expression

Photoreceptor and bipolar cells maintain OTX2 expression into adulthood (Fig. 7) (Beby and Lamonerie, 2013; Fossat et al., 2007; Nishida et al., 2003). Given the transient nature of the DHS-4D activity, other enhancers are needed to maintain *Otx2* in the adult retina. These likely contribute to the resilience and flexibility of OTX2 expression. Several potential *Otx2* enhancers have been described for the retina and other developing systems (Chan et al., 2020; Emerson and Cepko, 2011; Kurokawa et al., 2004, 2014; Muranishi et al., 2011; Perez-Cervantes et al., 2020; Wilken et al., 2015). For example, the DHS-2 and DHS-15 enhancers appear to mark OTX2+ cells during late development and in the maturing retina (Wilken et al., 2015). These enhancers overlap with elements O5 and O20, respectively, described by Chan and colleagues (Chan et al., 2020), who also introduce a previously undescribed enhancer, O7, which shows a similar expression pattern in the postnatal retina (Chan et al., 2020). It is likely that enhancers O7, DHS-2, DHS-15 and other elements regulate *Otx2* expression in photoreceptors and bipolar cells. Similar to *Otx2* initiation, this may involve redundant or compensatory mechanisms. We propose that retinal *Otx2* expression occurs in two phases: initiation and maintenance (Fig. 7). Once *Otx2* is initiated by DHS-4, OTX2 can then act in an autoregulatory fashion at other enhancers to maintain its expression through cell type-specific mechanisms in photoreceptors and bipolar cells. In support of this, OTX2 ChIP-sequencing shows OTX2 binding at the DHS-2, DHS-15 and O7 enhancers (Bunt et al., 2011; Samuel et al., 2014). Consistent with a role in initiation and not maintenance, no OTX2 binding was seen at the DHS-4D sequence (Fig. S13). The necessity of DHS-2, DHS-15, O7 and other putative *Otx2* maintenance enhancers and how they are regulated remains to be elucidated.

MATERIALS AND METHODS

Mice, electroporations and tissue collection

All animal experiments were conducted with approval from the University of Colorado Denver Institutional Animal Care and Use Committee. Male and female mice were used equally. Retinas were collected at either E14.5 or P0 from wild-type *CD1* (strain 022, Charles River Laboratories) or *ROSA-RFP* mice [*B6.Cg-Gt(ROSA)26Sor^{tm14}(CAG-tdTomato)Hze/J*] (strain 007914, Jackson Laboratories) (Madisen et al., 2010).

To screen enhancer activity, E14.5 or P0 retinas were dissected, electroporated and cultured as *ex vivo* explants as previously described (Mills et al., 2017). Briefly, eyes were dissected in cold Hank's Balanced Salt Solution (HBSS with Ca^{2+} and Mg^{2+}) (Corning) containing 6 mg/ml glucose and 0.05 M HEPES. P0 retinas were dissected free, whereas E14.5 eyes were dissected until only the retina and lens remained. Next, 1.5 µl of electroporation mix (45 µg of plasmid DNA dissolved in 9 µl of H_2O with 6 µl of methyl green in glycerol) was pipetted onto the photoreceptor side of the retinas. The retinas were electroporated with five square wave pulses of 50 V for 50 ms with 250 ms intervals (Bio-Rad Gene Pulser Xcell). The electroporated explants were then placed in growth media [Neurobasal Medium containing 1× N2 supplement, 1× L-glutamine, 1× penicillin/streptomycin and 1% fetal bovine serum (FBS)] (Gibco/Thermo Fisher Scientific) in a 12-well plate. Explants were cultured under 5% CO_2 in a 37°C incubator using a nutator (at 12 RPM) to oxygenate them gently for up to 72 h.

For *in vivo* electroporation, newborn *CD1* or *ROSA-RFP* mice were placed in a clear plastic bag on ice and cryo-anesthetized for 3-5 min. Once fully anesthetized and unresponsive to physical contact, mice were transferred to a solid ice pack, where they remained throughout the procedure. A 31G needle was used to create an incision lengthwise along the eyelid to expose the eye. A second 31G needle was inserted along the sclera nasally adjacent to the cornea to make a hole. A 32 g blunt tip Hamilton syringe, loaded with 0.5 µl of 2 µg/µl DNA in sterile H_2O, was inserted in the hole and the DNA was slowly injected into the subretinal space of the central retina. The positive electrode of a Tweezertrode (BTX) was placed over the eye containing the inserted DNA, whereas the negative end was placed on the opposing side of the head. Mice were electroporated with five 80 V square wave pulses for 50 ms with a 950 ms delay between each pulse using a Bio-Rad Gene Pulser Xcell. After electroporation, Neosporin was applied to the exterior of the eye and Buprenex (0.1 mg/kg) was given subcutaneously to minimize pain. Pups were then placed on a circulating water heating pad until recovered, and returned to their home cage.

Following culturing, explants destined for histology were fixed in 2% paraformaldehyde for 20 min at room temperature. Following *in vivo* electroporations, eyes were punctured with a 30 g needle in the cornea and fixed in 2% paraformaldehyde at room temperature for 1-2 h. After fixation, explants and eyes were cryopreserved through an increasing sucrose gradient (10%, 20%, 30%), frozen in OCT medium (Sakura) and stored at −80°C until they were cryosectioned.

Immunohistochemistry

Retinal tissues were cryosectioned at 10 µm on a Thermo Fisher Scientific MICROM HM 550 cryostat and immediately placed on Colorfrost Plus microscope slides (Thermo Fisher Scientific). Slides were incubated at room temperature for 1 h in milk block solution (the supernatant of 5% milk and 0.5% Triton X-100 in PBS) (Brzezinski et al., 2010). Primary antibodies were diluted in milk block and the slides incubated overnight (12-18 h) at room temperature. The slides were washed in PBS and incubated for 1 h at room temperature with fluorescently conjugated secondary antibodies (Jackson ImmunoResearch) diluted 1:500 in milk block solution. After another round of PBS washes, the slides were mounted. Primary antibodies used in this study were: mouse anti-ASCL1 (1:250; 556604, BD Biosciences) or rabbit monoclonal anti-ASCL1 (1:250; ab211327, Abcam), rabbit anti-AP2B (1:250; sc-8976, Santa Cruz Biotechnology), mouse anti-BRN3a (1:100; sc-8429, Santa Cruz Biotechnology), mouse anti-Ki67 (1:250; 550609, BD Biosciences), mouse anti-NEUROG2 (1:250; MAB3314, Santa Cruz Biotechnology), rabbit anti-OLIG2 (1:250; AB9610, Merck Millipore), goat anti-OTX2 (1:250; BAF1979, R&D Systems), rabbit anti-ONECUT1 (1:250; sc-13050, Santa Cruz Biotechnology), rabbit anti-PAX6 (1:250; 901301, BioLegend), mouse anti-RXRG (1:250; sc-514134, Santa Cruz Biotechnology), goat anti-SOX2 (1:250; sc-17320, Santa Cruz Biotechnology) and mouse anti-VSX2 (1:100; sc-374151, Santa Cruz Biotechnology). For visualizing plasmid-expressed fluorescent reporters, the GFP signal was enhanced

Development (2021) 148, dev199399. doi:10.1242/dev.199399

by staining with chicken anti-GFP (1:1000; ab13970, Abcam) and mCherry was detected with mouse anti-RFP (1:500; ab65856, Abcam). For explant EdU labeling, 1 µl of 10 mM EdU was added to 1 ml of warm media 30 min prior to fixation. Visualization of EdU incorporation was performed using the Click-iT™ EdU Imaging Kit (C10337, Thermo Fisher Scientific), after the secondary step, as described previously (Brzezinski et al., 2013; Goodson et al., 2020a; Kaufman et al., 2019).

Imaging and statistics

Images of retinal immunostaining were acquired using a Nikon C2 laser scanning confocal microscope. Images were captured as a 1024×1024 pixel area using each laser sequentially to generate the final image. Three to five *z*-stacks (1-1.5 µm per slice) were captured, maximum-intensity *z*-projected with ImageJ (Schneider et al., 2012) and minimally processed using Adobe Photoshop. Quantification of images was performed using the following workflow: Nikon ND2 stacks were imported into ImageJ, *z*-stacks were flattened and color channel levels were normalized. Cell counts were acquired manually, whereby each channel was visually inspected and labeled cell numbers were recorded in Microsoft Excel. All cells were identified in image regions of interest normalized to 250 µm of retinal length or per 200× field. For each experiment involving cell quantification, a minimum of three biological samples of mouse retinal explants or *in vivo* retinas were used. Two-tailed unpaired *t*-tests or one-way ANOVA were performed using Excel or GraphPad Prism 8; $P<0.05$ was considered to be significant.

Enhancer cloning and mutagenesis

The enhancer sequence for the full-length DHS-4 was obtained from Wilken et al. (2015). For all enhancer cloning, primers were designed against mouse mm10 GRCm38 genomic sequences and amplified from *C57BL/6J* mouse DNA (strain 664, Jackson Laboratories). Enhancer sequences were cloned into the pMin-nGFP plasmid, upstream of a minimal TATA promoter to drive the expression of nuclear GFP (Wilken et al., 2015). The plasmid was digested with *Eco*RI and *Kpn*I to linearize, followed by In-Fusion HD-based Gibson Assembly of various enhancer PCR fragments into the final plasmid product following the manufacturer's protocol (Takara Bio USA). Site-directed mutagenesis of E-box sites within the DHS-4 sub-element D (DHS-4D) enhancer was performed using inverse PCR amplification of the parent plasmid with primers incorporating the CANNTG to CANNAT mutation (Mills et al., 2017). A version of DHS-4D with all six E-boxes replaced by mutant CANNAT sequences was ordered as a gene block (Integrated DNA Technologies; IDT) to generate a fully mutant variant. In some cases, to speed construction, we used site-directed mutagenesis to revert mutated sites back to wild type. To generate lineage-tracing constructs, the pMin-nGFP vector (Wilken et al., 2015) was modified to co-express *Cre* recombinase (Goodson et al., 2020b). Briefly, the nuclear-localized GFP cassette was modified to include a P2A self-cleavage peptide sequence and a *Cre* recombinase cassette. As with the other constructs, In-Fusion cloning was used to insert *Otx2* enhancers into the *Eco*RI and *Kpn*I sites, generating DHS4-GFP-2A-Cre and DHS4D-GFP-2A-Cre plasmids. All enhancers and primer sequences are listed in Table S1. Base pMin plasmids driven by the whole DHS-4 and minimal DHS-4D elements were deposited in the Brzezinski Lab repository with Addgene (https://www.addgene.org/Joseph_Brzezinski/).

Design of CRISPR/Cas9 plasmids

The pSpCas9(BB)-2A-GFP (PX458) plasmid was acquired through Addgene (plasmid #48138) as a gift from Dr Feng Zhang (Massachusetts Institute of Technology, Cambridge, USA) (Ran et al., 2013). This plasmid was first modified by digesting with *Kpn*I and *Age*I and replacing the Cbh promoter with an EF1α promoter sequence PCR amplified from pLVX-mCherry (632561, Takara Bio USA). Second, the GFP reporter sequence was replaced with mCherry to establish a second reporter color. Finally, Histone H2B nuclear localization peptide was then added to each reporter variant. This resulted in both cytoplasmic (EF1α-pSpCas9-2A-GFP and EF1α-pSpCas9-2A-mCherry) and permanently nuclear-localizing (EF1α-pSpCas9-2A-H2B-GFP and EF1α-pSpCas9-2A-H2B-mCherry) versions of each variant. These newly generated plasmid backbones and nuclear reporter variants have been deposited with Addgene (#159654 and #159655 at https://www.addgene.org/Joseph_Brzezinski/).

To induce loss-of-function phenotypes, guide RNAs were designed to target protein-coding exon sequences for direct gene disruption or to flank crucial enhancer sequences. All guides were designed using the CRISPR Design and Analyze Guides tool, available through Benchling.com. On-target scores were ranked in descending order and guides with scores greater than 70 and off-target scores less than 50 were considered for use. Guides were submitted to BLAST and screened to identify any potential off-target effects on coding sequences. Three guides per target were selected and ordered as paired oligos from IDT. All guide sequences are listed in Table S1. CRISPR/Cas9 plasmid all-in-one reporter backbones created as described above were digested with *Bbs*I and used for Golden Gate cloning to insert annealed and phosphorylated guide oligos as detailed previously (Ran et al., 2013). Electroporations that targeted enhancer regions were always performed with all three guide plasmids. In the case of targeting coding regions, we found that two guides were sufficient. Therefore, we used two all-in-one CRISPR/Cas9 plasmids for these electroporations. For the *in vivo Ascl1/Neurog2* multiplexed experiment (Fig. 6) and the triple-gene knockout (*Ascl1*/*Neurog2*/*Olig2*)-targeting work (Fig. S9), we developed a new strategy to deliver two guides on a single plasmid. Using our modified PX458 backbone, we ligated a second U6 guide cassette into the *Xba*I and *Kpn*I restriction sites. A donor plasmid containing the U6 guide cassette was engineered to have compatible flanking *Xba*I and *Kpn*I restriction ends. This enabled a single all-in-one plasmid to target a coding region or enhancer with two flanking guides. Enhancer- and gene-targeting knockout constructs have been deposited with Addgene (#159656, #159657, #159658, #159659, #159660, #159661, #171101, #171098, #159662, #159663, #159664 and #171102 at https://www.addgene.org/Joseph_Brzezinski/).

Single cell RNA-sequencing library construction

Retinas from E14.5 CD-1 mice were harvested as above and electroporated with DHS-4D in pMin-nGFP and a ubiquitously expressed pLVX-H2B-mCherry plasmid construct. Retinas were placed in growth media and incubated as above until 16, 20 and 48 h post-electroporation. Retinas were dissociated with the Worthington Papain Dissociation System with some modifications (Worthington Biochemical Corporation). Briefly, up to five mouse embryonic retinas were added per activated Papain tube and incubated on a nutator at 37°C for 20-45 min. The dissociation status of the tissue was checked every 10 min and the cells gently triturated two to three times using a 1 ml pipette. Immediately prior to achieving a final single cell suspension, warmed DNase solution was added dropwise, gently inverted to mix and then incubated for 5 min on rotator at 37°C. Next, prewarmed ovomucoid solution was slowly added dropwise and again gently inverted to mix. Cells were spun down for 5 min at 300 ***g*** and the supernatant carefully aspirated. Cells were then resuspended and washed with 1% FBS+PBS (without calcium or magnesium). After washing, cells were spun for 5 min at 300 ***g*** and resuspended with 1% FBS+PBS for flow cytometry. FACS was performed with assistance from the Flow Cytometry Shared Resource (University of Colorado Cancer Center). GFP+ (± mCherry) and mCherry-only cells were separately collected in 10% FBS+PBS (without calcium or magnesium), counted on a hemocytometer and resuspended in 10% FBS+PBS. GFP+ (±mCherry) and mCherry-only cells were mixed at a 40/60 ratio and cell suspensions were then submitted to the University of Colorado Denver Anschutz Medical Campus Genomics and Microarray Core for droplet barcoding on the 10X Chromium using the Chromium Single Cell 3′ Reagent Kit V2 (10X Genomics).

Single cell RNA-sequencing analysis

Following barcoding, constructed libraries were sequenced on an Illumina NovaSEQ6000. Initial demultiplexing of raw base calls was conducted with Cell Ranger 2.2 (10X Genomics). The sequence for GFP was added to the mouse reference genome to enable alignment and detection of reads from the DHS-4D-GFP plasmid. Using cellranger mkfastq and cellranger counts, we completed alignment (mm10), filtering, barcode counting and unique molecular identifier (UMI) counting. Based on UMIs and following removal of doublets, we captured 1843 cells. Read depth was estimated

Development (2021) 148, dev199399. doi:10.1242/dev.199399

to be ~250K reads per cell. Further quality control, clustering and trajectory analyses were performed using the Scanpy 1.4.6 (https://github.com/theislab/scanpy) (Wolf et al., 2018) python package running in a JupyterLab 2.1.0 notebook. After quality control (removal of high mitochondrial representation and low number of genes detected), we used UMAP dimension reduction by Leiden-based clustering in the Scanpy Python package to identify 13 clusters using default parameters (McInnes et al., 2018; Wolf et al., 2018). The workflow pipeline was created by following and integrating steps within the pbmc3k, visualizing-marker-genes and paga-paul15 tutorials found within the Scanpy documentation site. We did not use regression to account for cell cycle or other state-like properties. Clusters were analyzed for, and visualized with, known cell type-specific marker signatures using the sc.tl.rank_genes_groups and sc.pl.rank_genes_groups_dotplot functions. Trajectory analysis was performed using the diffusion pseudotime (sc.tl.dpt) method in Scanpy (Haghverdi et al., 2016). Partition-based graph abstraction (sc.tl.paga) was used to align cells along a pseudotime path. Cells were then aligned according to their pseudotime score and plotted in ForceAtlas2 component space (sc.tl.draw_graph) and visualized with their original Leiden clusters (Jacomy et al., 2014). To identify candidate transcription factors, we isolated the pseudotime pathway that ends with cluster 12, which includes *Otx2*+ photoreceptors. Expression values of candidates were extracted from the temporally mapped diffusion pseudotime trajectories. Raw expression patterns along these trajectories for known genes and candidate bHLH genes were exported and plotted as a heatmap using Morpheus (https://software.broadinstitute.org/morpheus/). RNA-sequencing data are available at GEO under accession number GSE172101.

JASPAR transcription factor-binding predictions

The JASPAR 2020 database online tool (http://jaspar.genereg.net/) was used to identify potential transcription factor-binding sites in the DHS-4 sequence. bHLH transcription factor motifs (*Ascl1*, *Neurog2*, *Olig2*, *Neurod1*, *Neurod4* and *Bhlhe22*) were used for the scan. The analysis was run with a minimum score threshold of 80%. Binding-site maps were created using the BioPython package. A SeqRecord object was created in Genbank format using the enhancer DNA sequence and annotated with motif sites and scores from JASPAR. Colors represent percentiles above the 80% score threshold, with pure black being the highest score range (>95%). Output was saved as a Genbank file (.gb) and was imported into SnapGene Viewer (SnapGene) for visualization and creation of figure images. Custom code is available at https://github.com/MLKaufman/tfbs_annotate.

Visualization of external datasets

Genomic tracks were visualized using either the UCSC Genome Browser or the Integrative Genomics Viewer (Kent et al., 2002; Robinson et al., 2011). P0 mouse whole-retina ASCL1 ChIP-seq (Jorstad et al., 2020) data were used in Fig. S11. The following datasets were used in Fig. S13: 4- to 5-week-old mouse whole-retina ChIP-seq (Samuel et al., 2014), 8-week-old mouse whole-retina CRX ChIP-seq (Corbo et al., 2010) and E14, P0 and P21 mouse whole-retina ATAC-seq (Norrie et al., 2019).

Acknowledgements

The authors thank Tom Reh and Matt Wilken for helpful discussion about the roles of *Otx2* enhancers in the retina, and Ian Purvis and Omar Ochoa Olmos for critically reading the manuscript. The authors thank Katrina Diener and the CU Denver Genomics and Microarray Core for helpful discussions and technical assistance regarding 10X Genomics single cell RNA barcoding and high-throughput sequencing. The authors thank Dmitry Baturin and Lester Acosta of the CU Cancer Center Flow Cytometry for technical assistance with cell sorting. For guidance with analysis of the single cell RNA-sequencing data, we thank G. Devon Trahan.

Competing interests

The authors declare no competing or financial interests.

Author contributions

Conceptualization: M.L.K., J.A.B.; Methodology: M.L.K., N.B.G., K.U.P., M.S., E.O., S.R.S., J.A., A.H., K.L.J.; Software: M.L.K., K.L.J.; Formal analysis: M.L.K., K.L.J.; Investigation: M.L.K., N.B.G., K.U.P., M.S., E.O., S.R.S., J.A., A.H., K.L.J., J.A.B.; Resources: J.A.B.; Data curation: M.L.K.; Writing - original draft: M.L.K.; Writing - review & editing: M.L.K., N.B.G., K.U.P., M.S., E.O., S.R.S., J.A., A.H., K.L.J., J.A.B.; Visualization: M.L.K.; Supervision: J.A.B.; Project administration: J.A.B.; Funding acquisition: J.A.B.

Funding

Work was supported, in part, by grants from the National Institutes of Health (R01-EY024272 to J.A.B.; T32-NS099042 to N.B.G.) and by the National Center for Advancing Translational Sciences Colorado Clinical and Translational Science Awards Program (TL1 TR002533 to N.B.G.). A.H., E.O. and J.A. were supported by the Gates Summer Internship Program at the University of Colorado Denver. S.R.S. was supported by a Challenge Grant from the Boettcher Foundation. Work was partially supported by an Unrestricted Grant to the University of Colorado Department of Ophthalmology from Research to Prevent Blindness. Deposited in PMC for release after 12 months.

Data availability

RNA-sequencing data have been deposited in GEO under accession number GSE172101.

Peer review history

The peer review history is available online at https://journals.biologists.com/dev/article-lookup/doi/10.1242/dev.199399

References

Akagi, T., Inoue, T., Miyoshi, G., Bessho, Y., Takahashi, M., Lee, J. E., Guillemot, F. and Kageyama, R. (2004). Requirement of multiple basic helix-loop-helix genes for retinal neuronal subtype specification. *J. Biol. Chem.* **279**, 28492-28498. doi:10.1074/jbc.M400871200

Alexiades, M. R. and Cepko, C. (1996). Quantitative analysis of proliferation and cell cycle length during development of the rat retina. *Dev. Dyn.* **205**, 293-307. doi:10.1002/(SICI)1097-0177(199603)205:3<293::AID-AJA9>3.0.CO;2-D

Baas, D., Bumsted, K. M., Martinez, J. A., Vaccarino, F. M., Wikler, K. C. and Barnstable, C. J. (2000). The subcellular localization of Otx2 is cell-type specific and developmentally regulated in the mouse retina. *Brain Res. Mol. Brain Res.* **78**, 26-37. doi:10.1016/S0169-328X(00)00060-7

Bassett, E. A., Korol, A., Deschamps, P. A., Buettner, R., Wallace, V. A., Williams, T. and West-Mays, J. A. (2012). Overlapping expression patterns and redundant roles for AP-2 transcription factors in the developing mammalian retina. *Dev. Dyn.* **241**, 814-829. doi:10.1002/dvdy.23762

Beby, F. and Lamonerie, T. (2013). The homeobox gene Otx2 in development and disease. *Exp. Eye Res.* **111**, 9-16. doi:10.1016/j.exer.2013.03.007

Benoist, C. and Chambon, P. (1981). In vivo sequence requirements of the SV40 early promoter region. *Nature* **290**, 304-310. doi:10.1038/290304a0

Brown, N. L., Kanekar, S., Vetter, M. L., Tucker, P. K., Gemza, D. L. and Glaser, T. (1998). Math5 encodes a murine basic helix-loop-helix transcription factor expressed during early stages of retinal neurogenesis. *Development* **125**, 4821-4833. doi:10.1242/dev.125.23.4821

Brzezinski, J. A. and Reh, T. A. (2015). Photoreceptor cell fate specification in vertebrates. *Development* **142**, 3263-3273. doi:10.1242/dev.127043

Brzezinski, J. A., IV, Lamba, D. A. and Reh, T. A. (2010). Blimp1 controls photoreceptor versus bipolar cell fate choice during retinal development. *Development* **137**, 619-629. doi:10.1242/dev.043968

Brzezinski, J. A., IV, Kim, E. J., Johnson, J. E. and Reh, T. A. (2011). Ascl1 expression defines a subpopulation of lineage-restricted progenitors in the mammalian retina. *Development* **138**, 3519-3531. doi:10.1242/dev.064006

Brzezinski, J. A., IV, Uoon Park, K. and Reh, T. A. (2013). Blimp1 (Prdm1) prevents re-specification of photoreceptors into retinal bipolar cells by restricting competence. *Dev. Biol.* **384**, 194-204. doi:10.1016/j.ydbio.2013.10.006

Bunt, J., Hasselt, N. E., Zwijnenburg, D. A., Koster, J., Versteeg, R. and Kool, M. (2011). Joint binding of OTX2 and MYC in promotor regions is associated with high gene expression in medulloblastoma. *PLoS ONE* **6**, e26058. doi:10.1371/journal.pone.0026058

Carter-Dawson, L. D. and LaVail, M. M. (1979). Rods and cones in the mouse retina. II. Autoradiographic analysis of cell generation using tritiated thymidine. *J. Comp. Neurol.* **188**, 263-272. doi:10.1002/cne.901880205

Chan, C. S. Y., Lonfat, N., Zhao, R., Davis, A. E., Li, L., Wu, M.-R., Lin, C.-H., Ji, Z., Cepko, C. L. and Wang, S. (2020). Cell type- and stage-specific expression of Otx2 is regulated by multiple transcription factors and cis-regulatory modules in the retina. *Development* **147**, dev187922. doi:10.1242/dev.187922

Clark, B. S., Stein-O'Brien, G. L., Shiau, F., Cannon, G. H., Davis-Marcisak, E., Sherman, T., Santiago, C. P., Hoang, T. V., Rajaii, F., James-Esposito, R. E. et al. (2019). Single-cell RNA-seq analysis of retinal development identifies NFI factors as regulating mitotic exit and late-born cell specification. *Neuron* **102**, 1111-1126. doi:10.1016/j.neuron.2019.04.010

Corbo, J. C., Lawrence, K. A., Karlstetter, M., Myers, C. A., Abdelaziz, M., Dirkes, W., Weigelt, K., Seifert, M., Benes, V., Fritsche, L. G. et al. (2010). CRX ChIP-seq reveals the cis-regulatory architecture of mouse photoreceptors. *Genome Res.* **20**, 1512-1525. doi:10.1101/gr.109405.110

Ellenberger, T., Fass, D., Arnaud, M. and Harrison, S. C. (1994). Crystal structure of transcription factor E47: E-box recognition by a basic region helix-loop-helix dimer. *Genes Dev.* **8**, 970-980. doi:10.1101/gad.8.8.970

Emerson, M. M. and Cepko, C. L. (2011). Identification of a retina-specific Otx2 enhancer element active in immature developing photoreceptors. *Dev. Biol.* **360**, 241-255. doi:10.1016/j.ydbio.2011.09.012

Emerson, M. M., Surzenko, N., Goetz, J. J., Trimarchi, J. and Cepko, C. L. (2013). Otx2 and Onecut1 promote the fates of cone photoreceptors and horizontal cells and repress rod photoreceptors. *Dev. Cell* **26**, 59-72. doi:10.1016/j.devcel.2013.06.005

Fossat, N., Le Greneur, C., Béby, F., Vincent, S., Godement, P., Chatelain, G. and Lamonerie, T. (2007). A new GFP-tagged line reveals unexpected Otx2 protein localization in retinal photoreceptors. *BMC Dev. Biol.* **7**, 122. doi:10.1186/1471-213X-7-122

Ghinia Tegla, M. G., Buenaventura, D. F., Kim, D. Y., Thakurdin, C., Gonzalez, K. C. and Emerson, M. M. (2020). OTX2 represses sister cell fate choices in the developing retina to promote photoreceptor specification. *eLife* **9**, e54279. doi:10.7554/eLife.54279

Gillies, S. D., Morrison, S. L., Oi, V. T. and Tonegawa, S. (1983). A tissue-specific transcription enhancer element is located in the major intron of a rearranged immunoglobulin heavy chain gene. *Cell* **33**, 717-728. doi:10.1016/0092-8674(83)90014-4

Goodson, N. B., Kaufman, M. A., Park, K. U. and Brzezinski, J. A.IV. (2020a). Simultaneous deletion of Prdm1 and Vsx2 enhancers in the retina alters photoreceptor and bipolar cell fate specification, yet differs from deleting both genes. *Development* **147**, dev190272. doi:10.1242/dev.190272

Goodson, N. B., Park, K. U., Silver, J. S., Chiodo, V. A., Hauswirth, W. W. and Brzezinski, J. A.IV. (2020b). Prdm1 overexpression causes a photoreceptor fate-shift in nascent, but not mature, bipolar cells. *Dev. Biol.* **464**, 111-123. doi:10.1016/j.ydbio.2020.06.003

Hafler, B. P., Surzenko, N., Beier, K. T., Punzo, C., Trimarchi, J. M., Kong, J. H. and Cepko, C. L. (2012). Transcription factor Olig2 defines subpopulations of retinal progenitor cells biased toward specific cell fates. *Proc. Natl. Acad. Sci. USA* **109**, 7882-7887. doi:10.1073/pnas.1203138109

Haghverdi, L., Büttner, M., Wolf, F. A., Buettner, F. and Theis, F. J. (2016). Diffusion pseudotime robustly reconstructs lineage branching. *Nat. Methods* **13**, 845-848. doi:10.1038/nmeth.3971

Hatakeyama, J. and Kageyama, R. (2004). Retinal cell fate determination and bHLH factors. *Semin. Cell Dev. Biol.* **15**, 83-89. doi:10.1016/j.semcdb.2003.09.005

Hatakeyama, J., Tomita, K., Inoue, T. and Kageyama, R. (2001). Roles of homeobox and bHLH genes in specification of a retinal cell type. *Development* **128**, 1313-1322. doi:10.1242/dev.128.8.1313

Henke, R. M., Meredith, D. M., Borromeo, M. D., Savage, T. K. and Johnson, J. E. (2009). Ascl1 and Neurog2 form novel complexes and regulate Delta-like3 (Dll3) expression in the neural tube. *Dev. Biol.* **328**, 529-540. doi:10.1016/j.ydbio.2009.01.007

Hufnagel, R. B., Le, T. T., Riesenberg, A. L. and Brown, N. L. (2010). Neurog2 controls the leading edge of neurogenesis in the mammalian retina. *Dev. Biol.* **340**, 490-503. doi:10.1016/j.ydbio.2010.02.002

Jacomy, M., Venturini, T., Heymann, S. and Bastian, M. (2014). ForceAtlas2, a continuous graph layout algorithm for handy network visualization designed for the Gephi software. *PLoS ONE* **9**, e98679. doi:10.1371/journal.pone.0098679

Jorstad, N. L., Wilken, M. S., Todd, L., Finkbeiner, C., Nakamura, P., Radulovich, N., Hooper, M. J., Chitsazan, A., Wilkerson, B. A., Rieke, F. et al. (2020). STAT signaling modifies Ascl1 chromatin binding and limits neural regeneration from Muller Glia in adult mouse retina. *Cell Rep.* **30**, 2195-2208.e5. doi:10.1016/j.celrep.2020.01.075

Kataoka, H., Murayama, T., Yokode, M., Mori, S., Sano, H., Ozaki, H., Yokota, Y., Nishikawa, S. and Kita, T. (2000). A novel snail-related transcription factor Smuc regulates basic helix-loop-helix transcription factor activities via specific E-box motifs. *Nucleic Acids Res.* **28**, 626-633. doi:10.1093/nar/28.2.626

Kaufman, M. L., Park, K. U., Goodson, N. B., Chew, S., Bersie, S., Jones, K. L., Lamba, D. A. and Brzezinski, J. A.IV. (2019). Transcriptional profiling of murine retinas undergoing semi-synchronous cone photoreceptor differentiation. *Dev. Biol.* **453**, 155-167. doi:10.1016/j.ydbio.2019.05.016

Kent, W. J., Sugnet, C. W., Furey, T. S., Roskin, K. M., Pringle, T. H., Zahler, A. M. and Haussler, D. (2002). The human genome browser at UCSC. *Genome Res.* **12**, 996-1006. doi:10.1101/gr.229102

Koike, C., Nishida, A., Ueno, S., Saito, H., Sanuki, R., Sato, S., Furukawa, A., Aizawa, S., Matsuo, I., Suzuki, N. et al. (2007). Functional roles of Otx2 transcription factor in postnatal mouse retinal development. *Mol. Cell. Biol.* **27**, 8318-8329. doi:10.1128/MCB.01209-07

Kowalchuk, A. M., Maurer, K. A., Shoja-Taheri, F. and Brown, N. L. (2018). Requirements for Neurogenin2 during mouse postnatal retinal neurogenesis. *Dev. Biol.* **442**, 220-235. doi:10.1016/j.ydbio.2018.07.020

Kurokawa, D., Kiyonari, H., Nakayama, R., Kimura-Yoshida, C., Matsuo, I. and Aizawa, S. (2004). Regulation of Otx2 expression and its functions in mouse forebrain and midbrain. *Development* **131**, 3319-3331. doi:10.1242/dev.01220

Kurokawa, D., Ohmura, T., Sakurai, Y., Inoue, K., Suda, Y. and Aizawa, S. (2014). Otx2 expression in anterior neuroectoderm and forebrain/midbrain is directed by more than six enhancers. *Dev. Biol.* **387**, 203-213. doi:10.1016/j.ydbio.2014.01.011

la Vail, M. M., Rapaport, D. H. and Rakic, P. (1991). Cytogenesis in the monkey retina. *J. Comp. Neurol.* **309**, 86-114. doi:10.1002/cne.903090107

Long, H. K., Prescott, S. L. and Wysocka, J. (2016). Ever-changing landscapes: transcriptional enhancers in development and evolution. *Cell* **167**, 1170-1187. doi:10.1016/j.cell.2016.09.018

Madisen, L., Zwingman, T. A., Sunkin, S. M., Oh, S. W., Zariwala, H. A., Gu, H., Ng, L. L., Palmiter, R. D., Hawrylycz, M. J., Jones, A. R. et al. (2010). A robust and high-throughput Cre reporting and characterization system for the whole mouse brain. *Nat. Neurosci.* **13**, 133-140. doi:10.1038/nn.2467

Mao, C.-A., Wang, S. W., Pan, P. and Klein, W. H. (2008). Rewiring the retinal ganglion cell gene regulatory network: Neurod1 promotes retinal ganglion cell fate in the absence of Math5. *Development* **135**, 3379-3388. doi:10.1242/dev.024612

Maurer, K. A., Kowalchuk, A., Shoja-Taheri, F. and Brown, N. L. (2018). Integral bHLH factor regulation of cell cycle exit and RGC differentiation. *Dev. Dyn.* **247**, 965-975. doi:10.1002/dvdy.24638

McInnes, L., Healy, J., Saul, N. and Großberger, L. (2018). UMAP: uniform manifold approximation and projection. *J. Open Source Software* **3**, 861. doi:10.21105/joss.00861

Mills, T. S., Eliseeva, T., Bersie, S. M., Randazzo, G., Nahreini, J., Park, K. U. and Brzezinski, J. A.IV. (2017). Combinatorial regulation of a Blimp1 (Prdm1) enhancer in the mouse retina. *PLoS ONE* **12**, e0176905. doi:10.1371/journal.pone.0176905

Muranishi, Y., Terada, K., Inoue, T., Katoh, K., Tsujii, T., Sanuki, R., Kurokawa, D., Aizawa, S., Tamaki, Y. and Furukawa, T. (2011). An essential role for RAX homeoprotein and NOTCH–HES signaling in Otx2 expression in embryonic retinal photoreceptor cell fate determination. *J. Neurosci.* **31**, 16792-16807. doi:10.1523/JNEUROSCI.3109-11.2011

Murre, C., Bain, G., van Dijk, M. A., Engel, I., Furnari, B. A., Massari, M. E., Matthews, J. R., Quong, M. W., Rivera, R. R. and Stuiver, M. H. (1994). Structure and function of helix-loop-helix proteins. *Biochim. Biophys. Acta* **1218**, 129-135. doi:10.1016/0167-4781(94)90001-9

Nelson, B. R., Hartman, B. H., Ray, C. A., Hayashi, T., Bermingham-McDonogh, O. and Reh, T. A. (2009). Acheate-scute like 1 (Ascl1) is required for normal delta-like (Dll) gene expression and notch signaling during retinal development. *Dev. Dyn.* **238**, 2163-2178. doi:10.1002/dvdy.21848

Nishida, A., Furukawa, A., Koike, C., Tano, Y., Aizawa, S., Matsuo, I. and Furukawa, T. (2003). Otx2 homeobox gene controls retinal photoreceptor cell fate and pineal gland development. *Nat. Neurosci.* **6**, 1255-1263. doi:10.1038/nn1155

Norrie, J. L., Lupo, M. S., Xu, B., Al Diri, I., Valentine, M., Putnam, D., Griffiths, L., Zhang, J., Johnson, D., Easton, J. et al. (2019). Nucleome dynamics during retinal development. *Neuron* **104**, 512-528.e11. doi:10.1016/j.neuron.2019.08.002

Parras, C. M., Schuurmans, C., Scardigli, R., Kim, J., Anderson, D. J. and Guillemot, F. (2002). Divergent functions of the proneural genes Mash1 and Ngn2 in the specification of neuronal subtype identity. *Genes Dev.* **16**, 324-338. doi:10.1101/gad.940902

Pattyn, A., Guillemot, F. and Brunet, J.-F. (2006). Delays in neuronal differentiation in Mash1/Ascl1 mutants. *Dev. Biol.* **295**, 67-75. doi:10.1016/j.ydbio.2006.03.008

Perez-Cervantes, C., Smith, L. A., Nadadur, R. D., Hughes, A. E. O., Wang, S., Corbo, J. C., Cepko, C., Lonfat, N. and Moskowitz, I. P. (2020). Enhancer transcription identifies cis-regulatory elements for photoreceptor cell types. *Development* **147**, dev184432. doi:10.1242/dev.184432

Ran, F. A., Hsu, P. D., Wright, J., Agarwala, V., Scott, D. A. and Zhang, F. (2013). Genome engineering using the CRISPR-Cas9 system. *Nat. Protoc.* **8**, 2281-2308. doi:10.1038/nprot.2013.143

Rapaport, D. H. and Vietri, A. J. (1991). Identity of cells produced by two stages of cytogenesis in the postnatal cat retina. *J. Comp. Neurol.* **312**, 341-352. doi:10.1002/cne.903120303

Roberts, M. R., Hendrickson, A., McGuire, C. R. and Reh, T. A. (2005). Retinoid X receptor γ is necessary to establish the S-opsin gradient in cone photoreceptors of the developing mouse retina. *Invest. Ophthalmol. Vis. Sci.* **46**, 2897-2904. doi:10.1167/iovs.05-0093

Robinson, J. T., Thorvaldsdóttir, H., Winckler, W., Guttman, M., Lander, E. S., Getz, G. and Mesirov, J. P. (2011). Integrative genomics viewer. *Nat. Biotechnol.* **29**, 24-26. doi:10.1038/nbt.1754

Samuel, A., Housset, M., Fant, B. and Lamonerie, T. (2014). Otx2 ChIP-seq reveals unique and redundant functions in the mature mouse retina. *PLoS ONE* **9**, e89110. doi:10.1371/journal.pone.0089110

Sapkota, D., Chintala, H., Wu, F., Fliesler, S. J., Hu, Z. and Mu, X. (2014). Onecut1 and Onecut2 redundantly regulate early retinal cell fates during development. *Proc. Natl. Acad. Sci. USA* **111**, E4086-E4095. doi:10.1073/pnas.1405354111

Sato, S., Inoue, T., Terada, K., Matsuo, I., Aizawa, S., Tano, Y., Fujikado, T. and Furukawa, T. (2007). Dkk3-Cre BAC transgenic mouse line: a tool for highly efficient gene deletion in retinal progenitor cells. *Genesis* **45**, 502-507. doi:10.1002/dvg.20318

Schneider, C. A., Rasband, W. S. and Eliceiri, K. W. (2012). NIH Image to ImageJ: 25 years of image analysis. *Nature Meth.* **9**, 671-675. doi:10.1038/nmeth.2089

Semple-Rowland, S. L., Coggin, W. E., Geesey, M., Eccles, K. S., Abraham, L., Pachigar, K., Ludlow, R., Khani, S. C. and Smith, W. C. (2010). Expression characteristics of dual-promoter lentiviral vectors targeting retinal photoreceptors and Müller cells. *Mol. Vis.* **16**, 916-934.

Singh, G., Mullany, S., Moorthy, S. D., Zhang, R., Mehdi, T., Tian, R., Moses, A. M. and Mitchell, J. A. (2021). A flexible repertoire of transcription factor binding sites and diversity threshold determines enhancer activity in embryonic stem cells. *Genome Res.* **31**, 564-575. doi:10.1101/gr.272468.120

Tomita, K., Nakanishi, S., Guillemot, F. and Kageyama, R. (1996). Mash1 promotes neuronal differentiation in the retina. *Genes Cells* **1**, 765-774. doi:10.1111/j.1365-2443.1996.tb00016.x

Turner, D. L. and Cepko, C. L. (1987). A common progenitor for neurons and glia persists in rat retina late in development. *Nature* **328**, 131-136. doi:10.1038/328131a0

Turner, D. L., Snyder, E. Y. and Cepko, C. L. (1990). Lineage-independent determination of cell type in the embryonic mouse retina. *Neuron* **4**, 833-845. doi:10.1016/0896-6273(90)90136-4

Wang, J. C.-C. and Harris, W. A. (2005). The role of combinational coding by homeodomain and bHLH transcription factors in retinal cell fate specification. *Dev. Biol.* **285**, 101-115. doi:10.1016/j.ydbio.2005.05.041

Wilken, M. S., Brzezinski, J. A., La Torre, A., Siebenthall, K., Thurman, R., Sabo, P., Sandstrom, R. S., Vierstra, J., Canfield, T. K., Hansen, R. S. et al. (2015). DNase I hypersensitivity analysis of the mouse brain and retina identifies region-specific regulatory elements. *Epigenet. Chromatin* **8**, 8. doi:10.1186/1756-8935-8-8

Wolf, F. A., Angerer, P. and Theis, F. J. (2018). SCANPY: large-scale single-cell gene expression data analysis. *Genome Biol.* **19**, 15. doi:10.1186/s13059-017-1382-0

Wong, L. L. and Rapaport, D. H. (2009). Defining retinal progenitor cell competence in Xenopus laevis by clonal analysis. *Development* **136**, 1707-1715. doi:10.1242/dev.027607

Wu, F., Sapkota, D., Li, R. and Mu, X. (2012). Onecut 1 and Onecut 2 are potential regulators of mouse retinal development. *J. Comp. Neurol.* **520**, 952-969. doi:10.1002/cne.22741

Wu, F., Li, R., Umino, Y., Kaczynski, T. J., Sapkota, D., Li, S., Xiang, M., Fliesler, S. J., Sherry, D. M., Gannon, M. et al. (2013). Onecut1 is essential for horizontal cell genesis and retinal integrity. *J. Neurosci.* **33**, 13053-13065, 13065a. doi:10.1523/JNEUROSCI.0116-13.2013

Yamamoto, H., Kon, T., Omori, Y. and Furukawa, T. (2020). Functional and evolutionary diversification of Otx2 and Crx in vertebrate retinal photoreceptor and bipolar cell development. *Cell Rep.* **30**, 658-671.e5. doi:10.1016/j.celrep.2019.12.072

Young, R. W. (1985). Cell differentiation in the retina of the mouse. *Anat. Rec.* **212**, 199-205. doi:10.1002/ar.1092120215

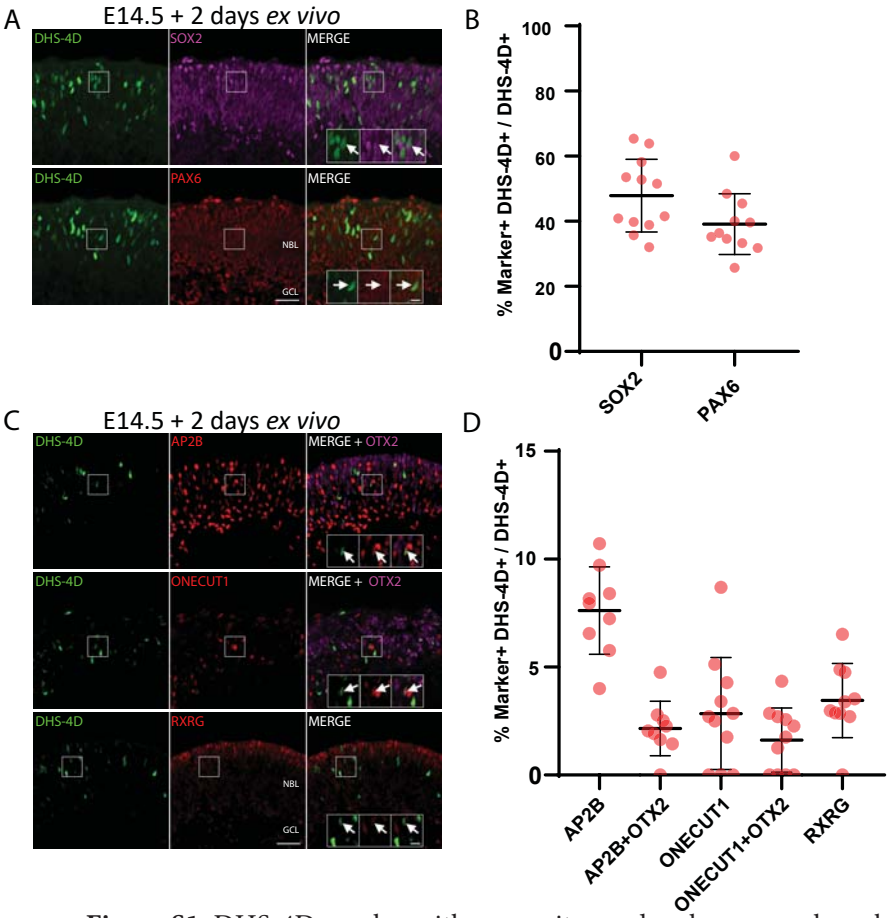

Figure S1: DHS-4D overlap with progenitor and early neuronal markers. (A) Representative histology of DHS-4D reporter electroporated into E14.5 retinal explants cultured for 2 days and stained for the progenitor markers SOX2 and PAX6. (B) Quantification of DHS- 4D overlap with SOX2 and PAX6. (C) Representative histology of DHS-4D reporter electroporated E14.5 explant retinas cultured for 2 days and stained for AP2B, ONECUT1, RXRG, and OTX2. (D) Quantification of DHS-4D overlap with AP2B, ONECUT1, RXRG, and triple overlap of AP2B and ONECUT1 with OTX2. Arrows mark double labeled cells in all panels. Dots represent quantified images from N=3 explants. NBL = neuroblastic layer, GCL = ganglion cell layer. Bars show the mean and s.d. Scale bars: 100μm; 25μm for insets.

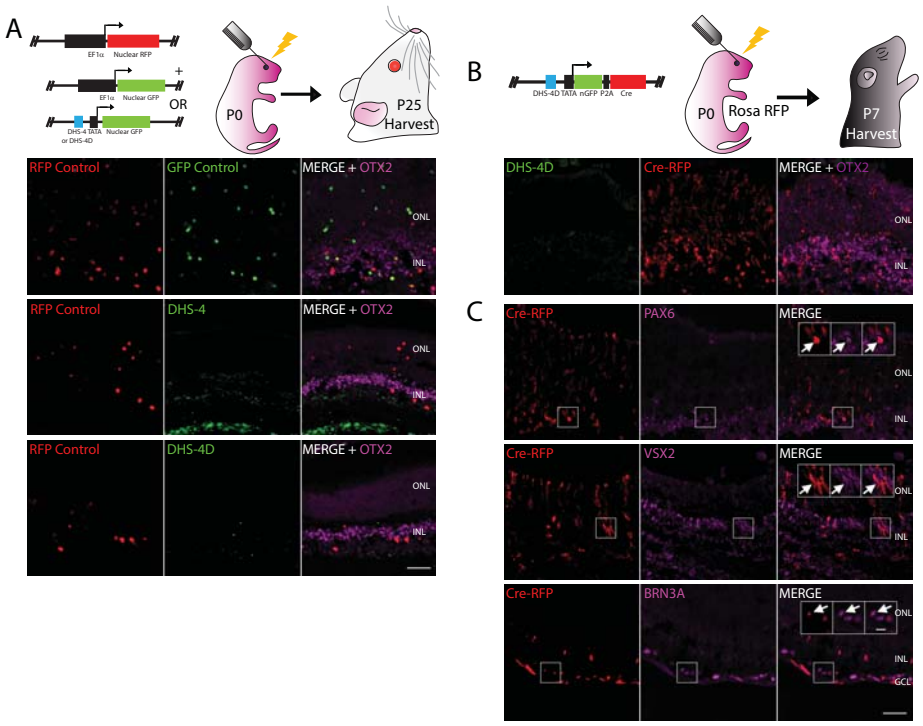

Figure S2: DHS-4 and DHS-4D long-term expression patterns. (**A**) Experimental design and histology of P0 CD1 mice electroporated in vivo with DHS-4, DHS-4D, or Control constructs harvested at P25. DHS-4 and DHS-4D lack activity in the mature retina. (**B**) Experimental design of lineage tracing utilizing DHS-4D driving GFP and P2A linked Cre. The plasmid was electroporated in vivo into P0 ROSA-RFP mice and the pups harvested at P7. (**C**) Histology of lineage traced mice stained for GFP, RFP, PAX6, VSX2, or BRN3A. DHS-4D lineage labeled cells (RFP+) contribute mostly to photoreceptor and bipolar cell fates. Arrows mark double labeled cells. ONL = outer nuclear layer, INL = inner nuclear layer, GCL = ganglion cell layer. Scale bars: 100μm; 25μm for insets.

A

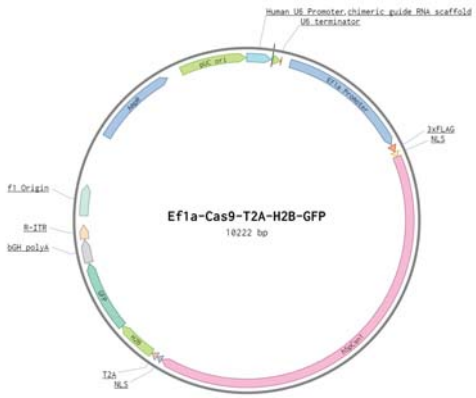

B

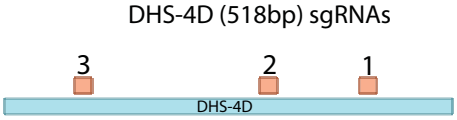

C

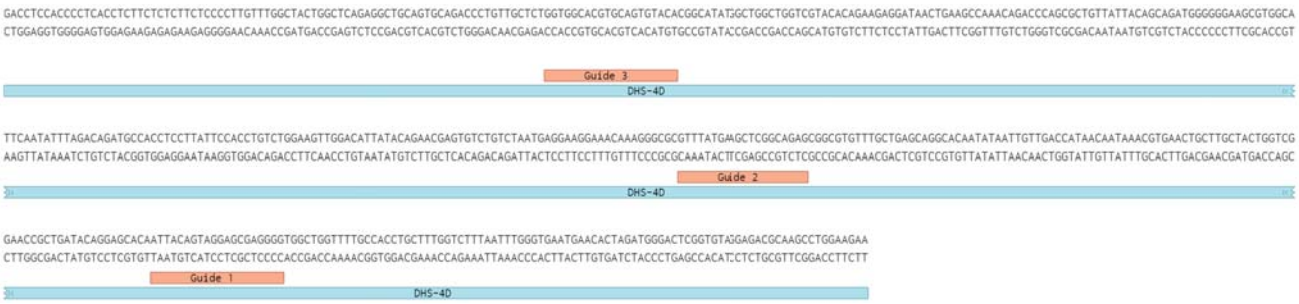

Figure S3: CRISPR/Cas9 DHS-4D knockout strategy. (A) Plasmid schematic of a modified PX458 CRISPR/Cas9 targeting construct. (B) Relative locations of CRISPR/Cas9 guides targeting DHS-4D. (C) Sequence base pair level location of CRISPR/Cas9 guides targeting DHS-4D.

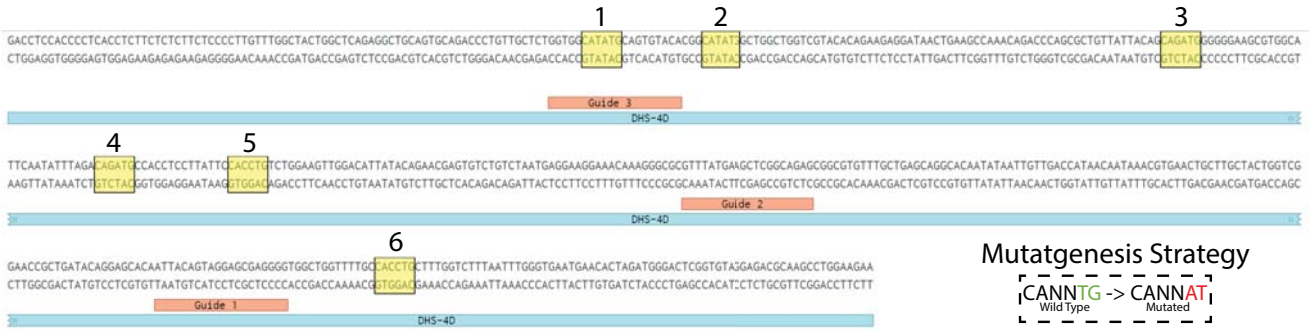

Figure S4: E-box sites within DHS-4D and the mutagenesis strategy. Locations and numbering of the six canonical CANNTG E-box sites identified relative to CRISPR/Cas9 guides. Mutagenesis strategy shown for reference.

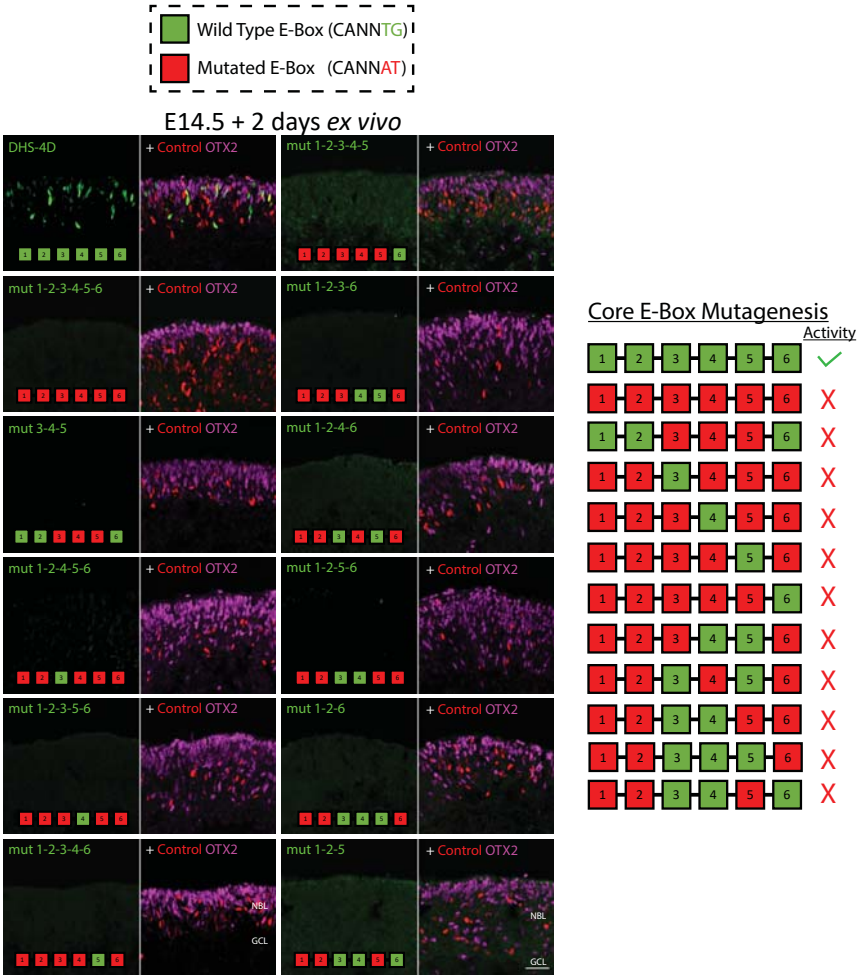

Figure S5: Core E-box mutagenesis series. Representative histology and summary of activity displayed by each mutant construct in the DHS-4D Core E-box mutagenesis strategy. E14.5 explants were electroporated and analyzed after two days of culture. Explants are stained for OTX2, GFP, and RFP. The X marks indicate constructs that lack activity or specificity. NBL = neuroblastic layer, GCL = ganglion cell layer. Scale bars = 100μm.

A

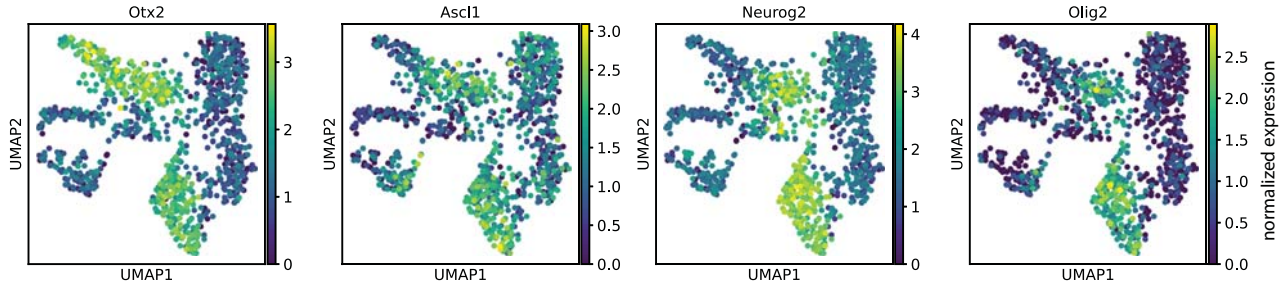

B

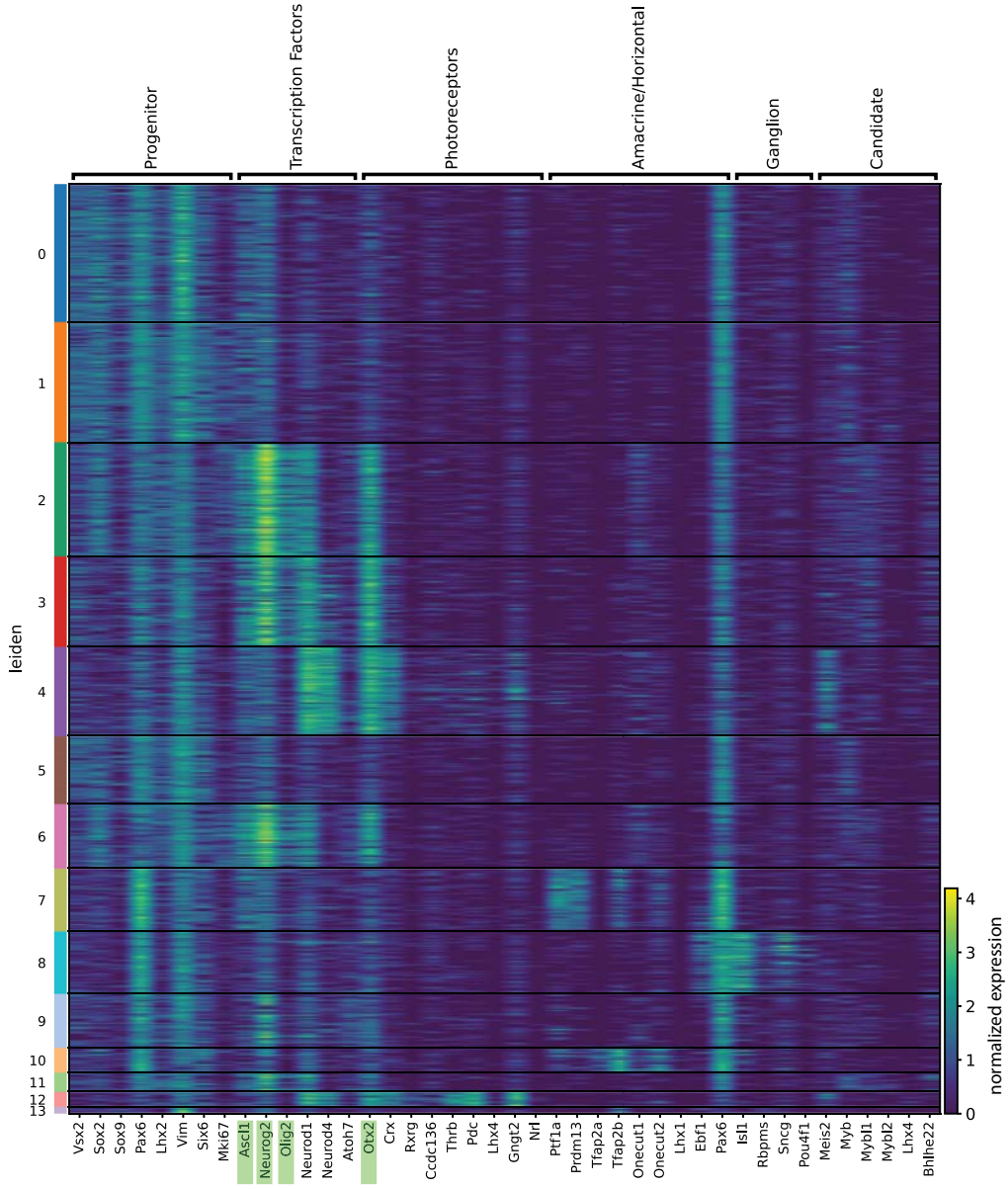

Figure S6: Additional single cell RNA sequencing findings. (A) UMAP plots with normalized expression values of *Otx2*, *Ascl1*, *Neurog2*, and *Olig2*. Note the high degree of overlap between these four transcription factors in UMAP space. (B) Heatmap representation of normalized expression of known marker genes and candidate transcription factor genes across leiden clusters. *Otx2*, *Ascl1*, *Neurog2*, and *Olig2* highlighted for reference.

A

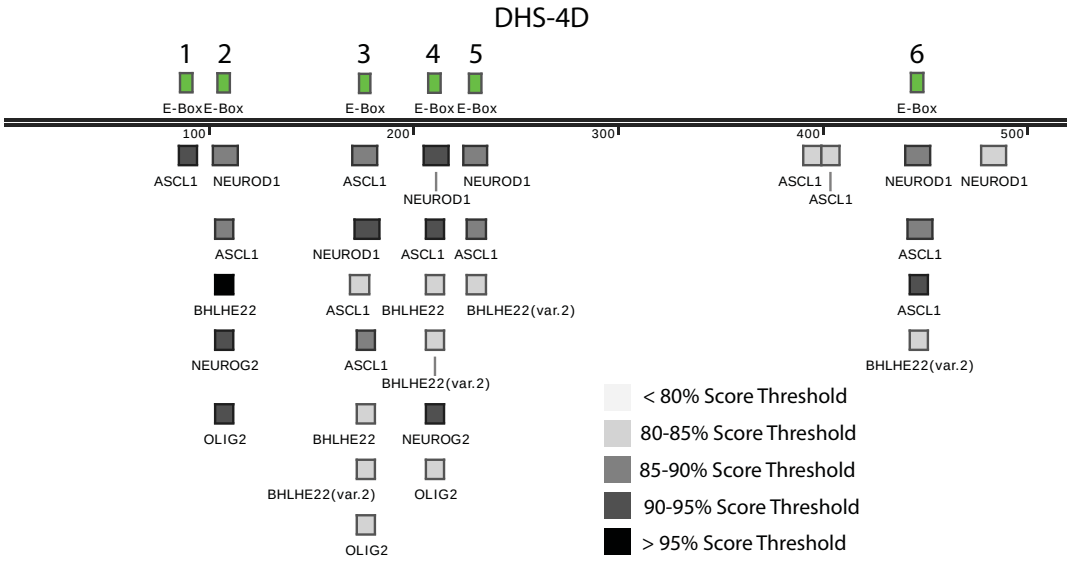

Figure S7: JASPAR transcription factor binding site analysis of DHS-4D. (A) Results of JASPAR transcription factor binding site analysis for bHLH transcription factors on the DHS-4D sequence. E-box placement and numbering are shown for reference. Grayscale gradient of transcription factors represents the JASPAR score threshold.

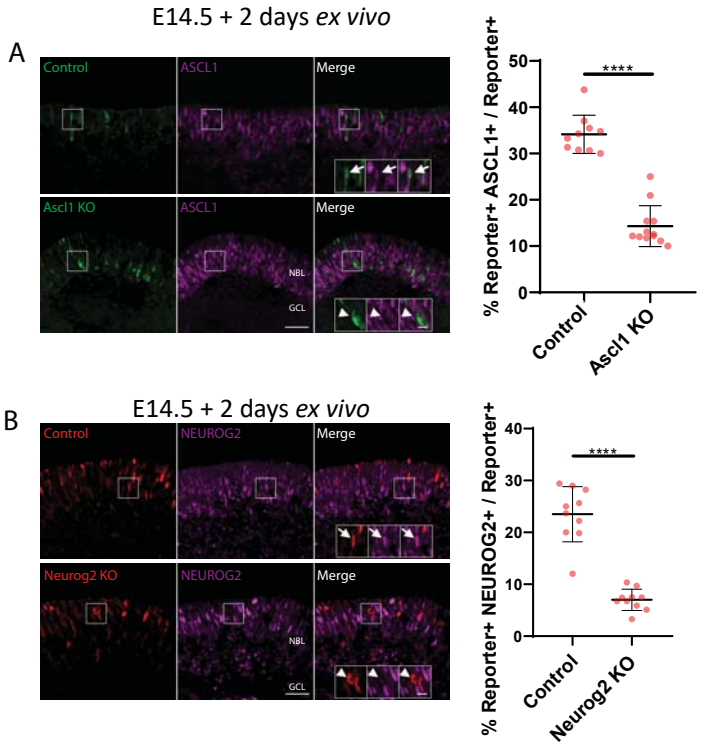

Figure S8: Ascl1 and Neurog2 CRISPR/Cas9 targeting efficiency. (A, B) Representative histology and quantification of non-targeting Controls and either Ascl1 or Neurog2 targeting CRISPR/Cas9 constructs. E14.5 retinas were electroporated with the constructs, grown in culture for two days, and stained for GFP, RFP, ASCL1 or NEUROG2. Arrows mark double labeled cells and arrowheads indicate singly labeled cells. Ascl1 and Neurog2 targeting constructs strongly reduce co-expression with ASCL1 and NEUROG2 proteins compared to Controls. Dots represent quantified images from N=3 retinas. NBL = neuroblastic layer, GCL = ganglion cell layer. Significance determined by two-tailed unpaired t-test. ****P<0.0001. Bars show the mean and s.d. Scale bars: 100μm; 25μm for insets.

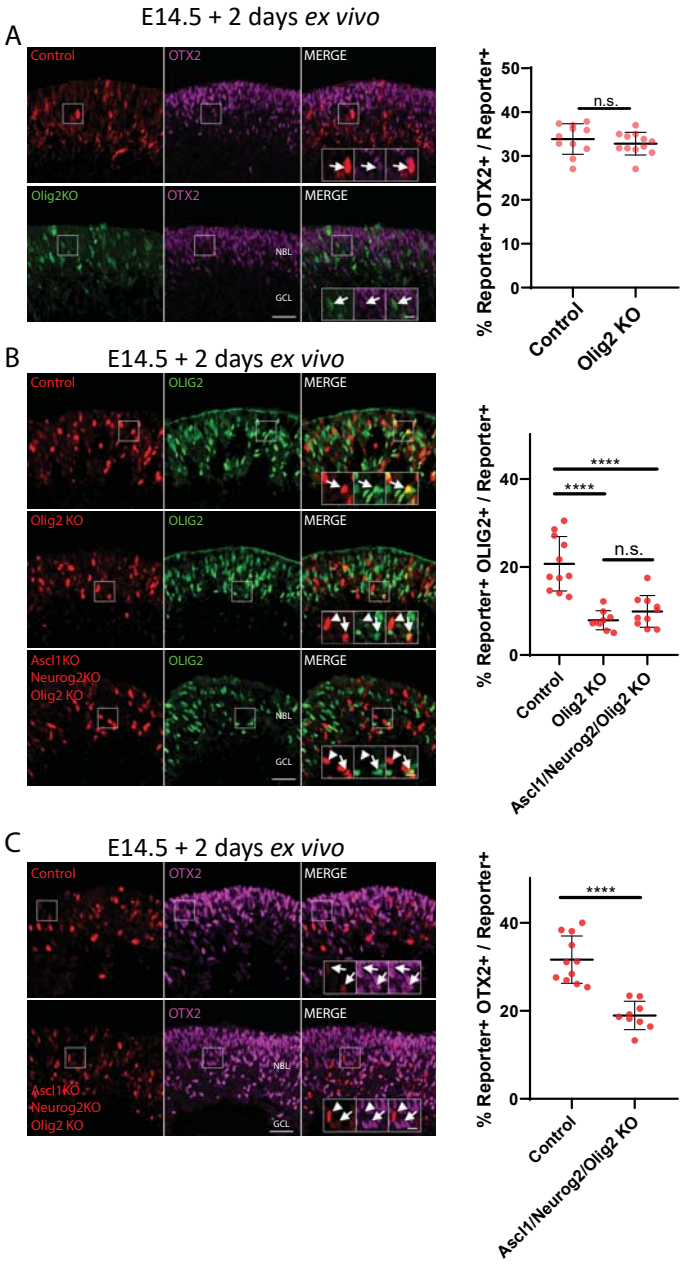

Figure S9: CRISPR/Cas9 knockout of *Olig2* does not inhibit OTX2 expression. (A) Representative histology and quantification of non-targeting Control and *Olig2* targeting CRISPR/Cas9 constructs electroporated into E14.5 retinal explants and cultured for two days. Sections are stained for GFP, RFP, or OTX2. Arrows mark electroporated cells that co-express OTX2. Dots represent quantified images from N=3 retinas. Comparison by two-tailed unpaired t-test. n.s = not significant. (B) Representative histology and quantification of E14.5 retinal explants electroporated with non-targeting Control, *Olig2* targeting, and triple *Ascl1/ Neurog2/Olig2* targeting constructs on OLIG2 expression. Sections are stained for RFP and OLIG2. Comparison by one-way ANOVA. n.s = not significant, ****P<0.0001. Targeting *Olig2* in isolation or as a combination has the same effect on reducing in the number of electroporated OLIG2+ cells. (C) Representative histology and quantification of E14.5 retinal explants electroporated with non-targeting Control and triple *Ascl1/Neurog2/Olig2* targeting constructs on OTX2 expression. Comparison by two-tailed unpaired t-test. n.s = not significant, ****P<0.0001. The triple targeting reduces OTX2 expression in electroporated cells as expected. This reduction is no greater than when *Ascl1* and *Neurog2* are co-targeted (see Figure 5B). Bars show the mean and s.d. NBL = neuroblastic layer, GCL = ganglion cell layer. Scale bars: 100μm; 25μm for insets.

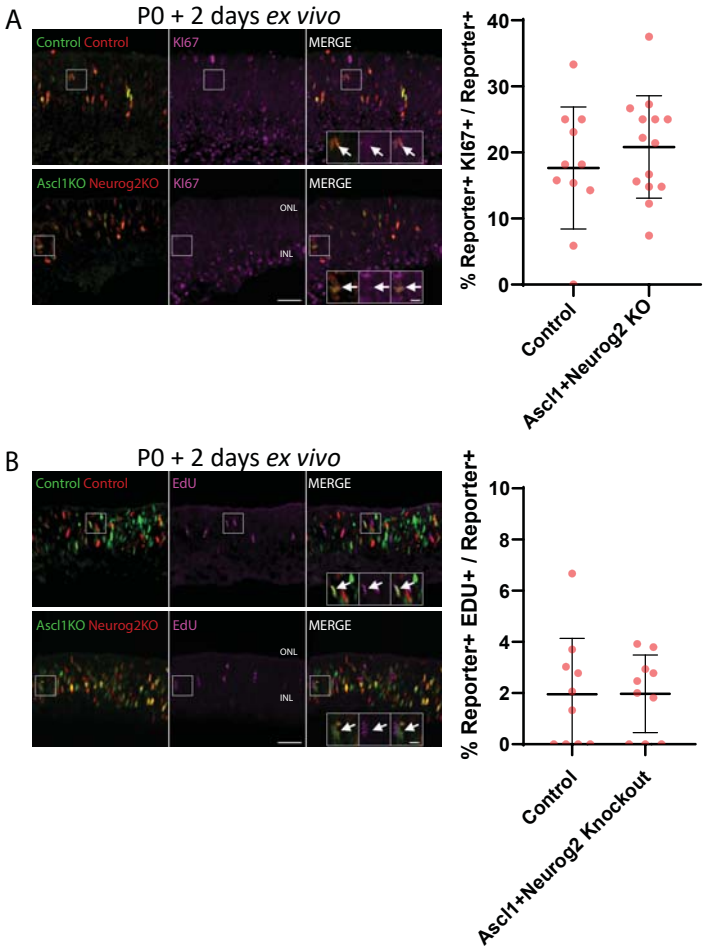

Figure S10: KI67 and EdU labeling is unchanged following Ascl1/Neurog2 double knockout. (A, B) Representative histology and quantification of non-targeting Controls and Ascl1/Neurog2 double targeting CRISPR/Cas9 constructs electroporated at E14.5 and collected after two days of culture. Sections are stained for GFP, RFP, Ki67 or EdU (given 30 minutes before collection). Arrows mark electroporated cells that co-express Ki67 or EdU. Dots represent quantified images from N=3 retinas. Bars show the mean and s.d. ONL = outer nuclear layer, INL = inner nuclear layer. Scale bars: 100μm; 25μm for insets.

A

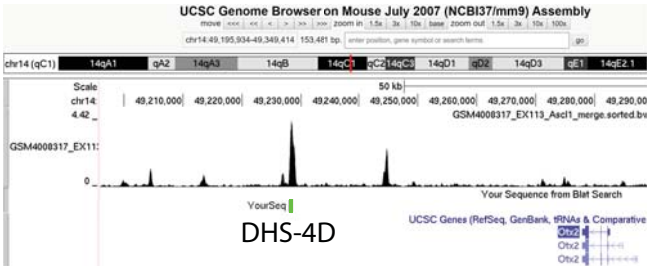

B

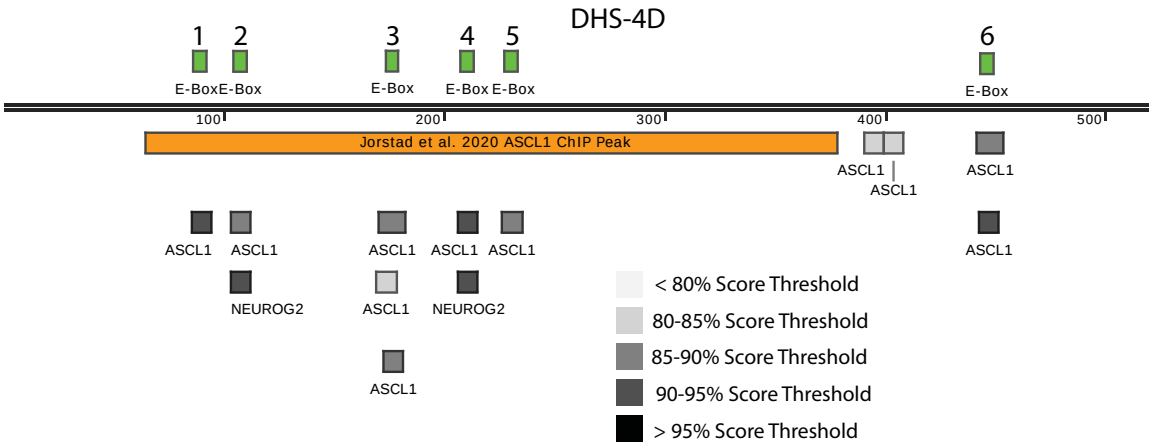

Figure S11: ASCL1 likely binds DHS-4D in the newborn retina. (A) Screenshot of the UCSC Genome Browser displaying the P0 retina ASCL1 ChIP-seq track from Jorstad et al. with DHS-4D highlighted (YourSeq) in green. There is a prominent ASCL1 peak centered on DHS-4D. (B) The DHS-4D sequence with JASPAR identified ASCL1 and NEUROG2 binding sites, numbered CANNTG E-Boxes, and the footprint of the Jorstad et al. ASCL1 ChIP-seq peak in orange. It is likely that ASCL1 binds one or more of the E-boxes in DHS-4D.

A

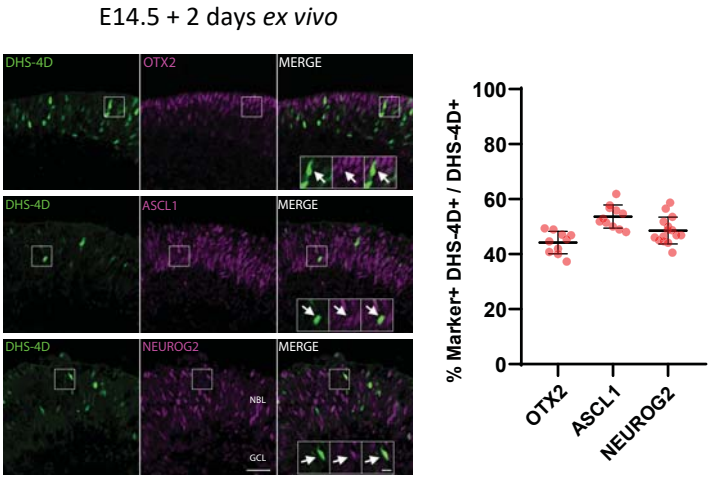

Figure S12: DHS-4D overlaps with ASCL1 and NEUROG2. (A) Histology and quantification of E14.5 retinal explants electroporated with DHS-4D TATA GFP constructs collected after 2 days of culture. Panels show co-staining of GFP with OTX2, ASCL1, or NEUROG2. About half of the GFP+ cells co-express ASCL1 or NEUROG2. N=3 retinas. Bars show the mean and s.d. NBL = neuroblastic layer, GCL = ganglion cell layer. Scale bars: 100μm; 25μm for insets.

A

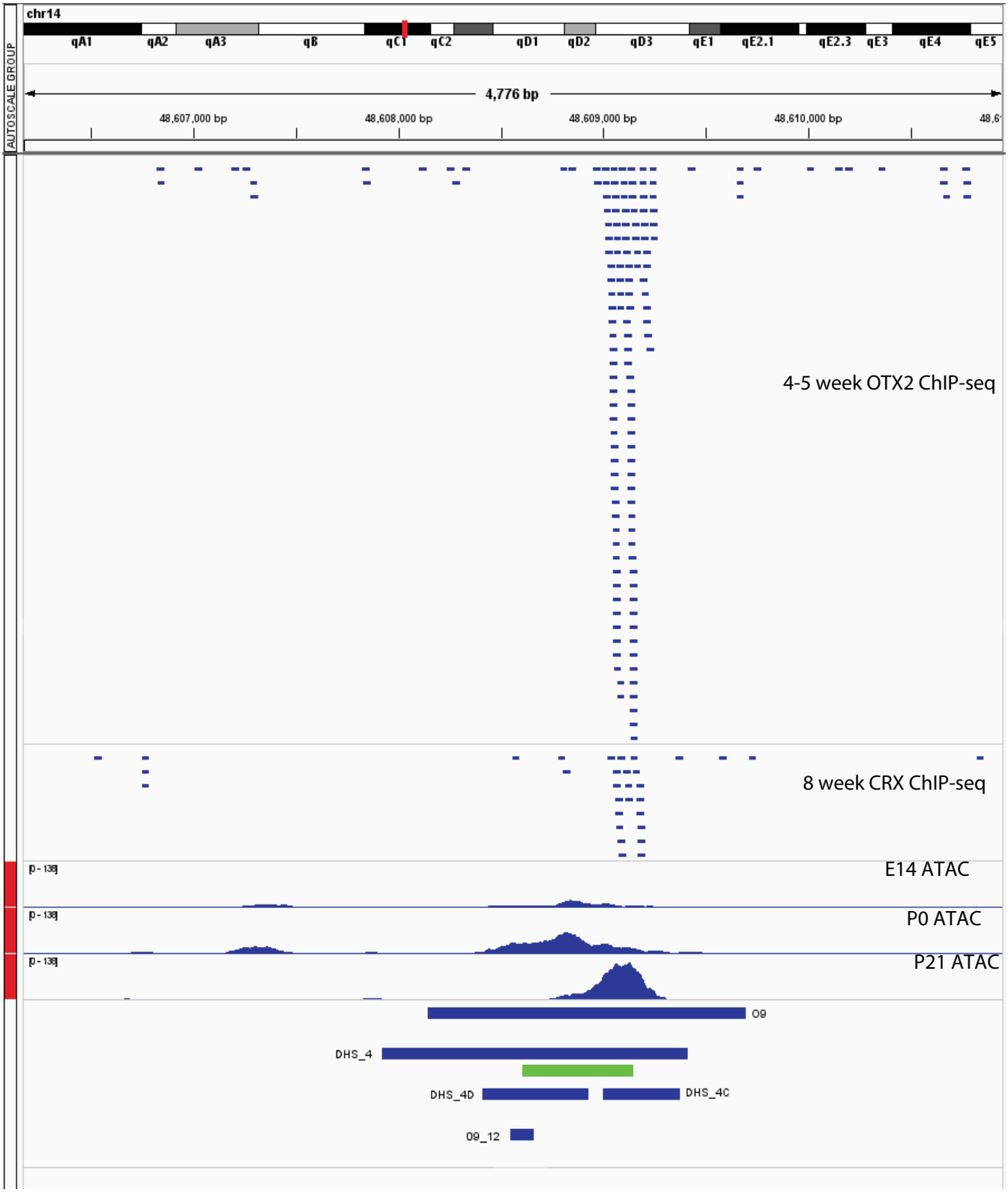

Figure S13: ATAC-seq and ChIP-seq peaks near the DHS-4 enhancer sequence region. (A) Screenshot of the IGV Genome Browser at the DHS-4 enhancer sequence. Tracks include 4-5 week old mouse whole retina OTX2 ChIP-seq, 8 week old mouse whole retina CRX ChIP-seq, and E14/P0/P21 mouse whole retina ATAC-seq. Below are the DHS-4, DHS-4D, DHS-4C, 09, and 09_12 enhancer elements for reference. OTX2 and CRX do not appear to bind in the DHS-4D region.

Table S1: Relevant sequences. Sequence list for DHS-4, sub-elements and CRISPR/ Cas9 targeting guide RNAs.

Click here to download Table S1